12-1-2016

Assessing a Potential Paleothermal Anomaly near a Salt Wall Using (U-TH)/HE Thermochronology and Silica Cementation Analysis, Onion Creek, Utah

Richard Gregory Ness
University of Nevada, Las Vegas

ASSESSING A POTENTIAL PALEOTHERMAL ANOMALY NEAR A SALT WALL USING (U-TH)/HE THERMOCHRONOLOGY AND SILICA CEMENTATION ANALYSIS, ONION CREEK, UTAH

By

Richard Gregory Ness

Bachelor of Science - Geology
University of Tennessee
2014

A thesis submitted in partial fulfillment of the requirements for the

Master of Science – Geoscience

Department of Geoscience
College of Sciences
The Graduate College

University of Nevada, Las Vegas
December 2016

UNLV | GRADUATE COLLEGE

Thesis Approval

The Graduate College
The University of Nevada, Las Vegas

November 16, 2016

This thesis prepared by

Richard Gregory Ness

entitled

Assessing a Potential Paleothermal Anomaly near a Salt Wall Using (U-TH)/HE Thermochronology and Silica Cementation Analysis, Onion Creek, Utah

is approved in partial fulfillment of the requirements for the degree of

Master of Science - Geoscience
Department of Geoscience

Andrew Hanson, Ph.D.
Examination Committee Chair

Kathryn Hausbeck Korgan, Ph.D.
Graduate College Interim Dean

Terry Spell, Ph.D.
Examination Committee Member

Wanda Taylor, Ph.D.
Examination Committee Member

Andrew Andres, Ph.D.
Graduate College Faculty Representative

ABSTRACT

The Onion Creek salt wall in Fisher Valley, Utah is an exposed salt structure that lies adjacent to sandstones of the Permian age Cutler Group. The thermal conductivity of salt is two to four times greater than other sedimentary rocks and has been shown to act as a regional conduit for heat flow which has implications for petroleum systems in hydrocarbon exploration. Numerical models predict that thermal anomalies should extend 1.5 times the radius of a salt structure into adjacent strata. I hypothesized that an elevated paleothermal anomaly exists in sandstones of the Cutler Group where they are located near the top of the salt wall. If the hypothesis is correct, thermochronologic ages should increase as distance from the salt wall increases because of elevated temperatures near salt. Additionally, the occurrence of silica cements should decrease with increasing distance away from salt. Apatite/zircon-He ages were determined for nine samples to test for a paleothermal anomaly. I also conducted an analysis of cementation in samples collected along a transect perpendicular to the salt wall. Apatite-He ages range from 33.3 ± 0.8 Ma to 17.9 ± 3.5 Ma and zircon-He ages range from 721 ± 15 Ma to 204 ± 147 Ma. Few silica cements were observed in the samples and the vast majority of cements are calcite which have no implications for paleotemperatures. The data show no definitive evidence for a paleothermal anomaly in the Cutler Group based on either the thermochronologic ages or the cementation analysis. I infer that both thermohaline convection of pore fluids and heterogeneous salt wall compositions may have masked the presence of a thermal anomaly if one existed. Apatite-He ages are reset but uniquely old given their location within the Colorado Plateau and suggest exhumation due to uplift associated with emplacement of the La Sal laccolith (~ 25 Ma). Zircon-He ages reflect exhumation in the Neoproterozoic possibly related to rifting of the supercontinent Rodinia.

ACKNOWLEDGMENTS

Thanks to Andrew Hanson for taking me on as a student. It's been a pleasure working with you and having the opportunity to learn about sedimentary basins (which are incredibly cool).

Special thanks to Wanda Taylor and Terry Spell for giving me back comments, helping me learn in their classes, and spending time in their offices answering my questions about low temperature thermochronology.

Thanks to Michael Wells for offering his class on the Geology of Western North America. That was a life changing class for me.

Thanks to ExxonMobil Production/Development and Upstream Research Companies for giving me the opportunity to be a professional geologist.

DEDICATION

"Geologists go where the rocks are. The rocks are not always in easy places. And, unlike tourists, who usually accept much of what they are told on their fleeting visit, geologists continually observe and ask questions, getting under the skin of the landscape they study. Ideally, a geologist would like to be able to flit from one place to another with an all-seeing eye, effortlessly taking in the key observations. Reality is very different. Much of your time is spent just getting around. And often you have no clear idea of where to look, or even, sometimes, what you are looking for. But somehow, if you persevere, the observations start to create patterns or ideas in the mind, and these grow and grow until you seem to be involved in a curious dialogue: *the rocks speak, you reply with a question, and they answer back.*"

Simon Lamb - *Devil in the Mountain*

This work is dedicated to Alissa Phillips and my mother, father, and sister. Thank you all for supporting me and believing in me when I, at times, did not believe in myself.

Also a special thanks to my Higher Power. Sometimes my Higher Power speaks through rocks.

TABLE OF CONTENTS

LIST OF TABLES

LIST OF FIGURES

CHAPTER 1: INTRODUCTION

1.1 Numerical Modeling of Salt Thermal Anomalies

Multiple numerical modeling studies have assessed heat flow from the base of a salt structure to its crest and within stratigraphy adjacent to salt (Selig & Wallick, 1966; Geertsma, 1971; Jensen, 1983; O'Brien & Lerche, 1984; Petersen & Lerche, 1995; Nagihara et al., 2003). The ability of salt to conduct heat into adjacent sedimentary rocks is important for applications in geothermal and hydrocarbon exploration (Rashid & McAlary, 1977; Vizgirda et al., 1985; Mello et al., 1995). Importantly, the thermal conductivity of rock salt is roughly two to four times higher than typical sedimentary rocks and is a more efficient conductor of heat than most other rock types (Fig. 1) (Petersen & Lerche, 1995; Mellow et al., 1995). Sedimentary rocks are generally considered to be poor conductors of heat, but when salt is present in a sedimentary basin it changes the geothermal gradient (Mello et al., 1995). Results from computer models suggest that subsurface isotherms are suppressed or elevated in the presence of salt. This change occurs because salt conducts heat upwards away from the base of a salt structure and focuses heat at the top of a salt structure (Fig.2) (Vizgirda et al., 1985). Consequently, heat transport from the base of a salt structure to its crest produces suppressed isotherms at depth and elevated isotherms at shallower levels within adjacent strata (Jensen, 1983; Vizgirda et al., 1985; Mello et al., 1995). If these models are correct, strata above or near the top of a salt structure may have above average temperatures while rocks below or at the base have cooler than average temperatures. Elevated temperature anomalies in strata directly above and adjacent to buried salt structures are modeled to be ~ 30˚C greater than regional temperatures based on burial depth alone in the absence of salt (Vizgirda et al., 1985; Yu et al., 1992). Models also predict that thermal anomalies should symmetrically extend into adjacent strata by roughly 1–1.5 times the radius of the salt structure assuming conduction of heat alone by salt (Petersen & Lerche, 1995).

Additionally, numerical models of salt temperature anomalies suggest that the only controls on the magnitude and extent of a salt thermal anomaly are the great thermal conductivity contrast between salt and sedimentary rocks, the shape of a salt body, and width of a salt structure. Numerical simulations also argue that the effects of fluid flow in strata adjacent to salt have such a small impact on modeled temperature anomalies that they are negligible (Yu et al., 1992).

1.2 Previous Assessment of an Exposed Paleothermal Anomaly

Published numerical models provide important understanding into heat flow within salt, but data that tests the presence, extent, and scale of salt paleothermal anomalies are rare. Recent work by Hanson (2014) in La Popa basin, Mexico demonstrates that salt thermal anomalies may be more complex than indicated by numerical simulations. Hanson (2014) collected thirty-seven mudstone samples from the same stratigraphic horizon within the uppermost Lower Mudstone Member of the Potrerillos Formation. The El Gordo salt diapir intersects the Potrerillos Formation to the northeast of the minibasin where a high density of samples were taken. Vitrinite reflectance data (R_o) of the mudstones indicate high thermal maturation values in the Potrerillos mudstones adjacent to the El Gordo diapir to the northwest and low thermal maturation values in mudstones adjacent to the diapir to the southeast (Fig. 3) (Hanson, 2014). These results suggest that the El Gordo diapir has an asymmetrical paleothermal anomaly that is five times the radius of the salt structure on one side and less than one radius on the other side. Two explanations for the asymmetry in thermal maturation values are that the diapir may either plunge to the northwest or has a zone of focused heat flow along the northwest margin of the salt structure. These data provide much needed characterization of an actual thermal anomaly in the field and point to the need for further work to integrate salt thermal modeling with results from field studies.

1.3 Silica Cementation and Salt Thermal Anomalies

The precipitation of silica cements and reduction of porosity in sandstones is a temperature dependent process. Thermal anomalies associated with salt structures theoretically extend into adjacent stratigraphy which are typically interbedded sandstones and shales. The temperature effects of a thermal anomaly associated with salt should impact the formation of silica cements in sandstones adjacent to salt. Decreases in sandstone porosity with increasing burial depth and thermal maturity is well established (Bjorlykke et al., 1986; Land & Fisher, 1987; Schmoker & Gautier, 1988). Typically, the most abundant cement in sandstones are silica cements which precipitate in sandstone pore spaces. Sources of silica for cements in sandstones vary depending on the sedimentary basin but can originate from dissolution and alteration of feldspars or by pressure solution of detrital quartz at styolites (Bjorlykke et al., 1986; McBride 1989; Walderhaug, 1994). Schomoker and Gautier (1988) demonstrate the dependence of sandstone porosity loss as a function of time exposure to elevated temperatures (Fig 4). Elevated temperatures initiate quartz cementation that is considered to be the most important factor behind reservoir quality degradation and porosity losses (Bjorlykke et al., 1986; McBride 1989; Walderhaug, 1994). Minor quartz cementation begins at a burial depth of 1 to 2 km at a temperature of 50˚C and the bulk of silica cementation occurs at 80˚C (McBride, 1989). As temperatures reach 80˚C in a sandstone, pore fluids saturated with silica begin to precipitate quartz cements on the surfaces of preexisting grain boundaries. Quartz cements continue to crystallize into pore space thereby reducing sandstone porosity and permeability.

Temperature anomalies in stratigraphy near the top of salt structures can be ~ 30˚C hotter than rocks farther away from salt under the influence of a normal geothermal gradient alone (Vizgirda et al., 1985; Yu et al., 1992). The presence of silica cements can be used as a proxy

for thermal maturity in sandstones. Therefore a study of silica cementation may test whether a thermal anomaly was present in sandstones adjacent to a salt structure. Increased amounts of quartz cement in sandstones located close to a salt structure versus reduced quartz cement farther from a salt structure would indicate an elevated temperature anomaly associated with heat flow within salt.

1.4 Low Temperature Thermochronology

Because of its temperature dependence, the use of (U-Th)/He thermochronology can potentially be an independent and novel test of a paleothermal anomaly in sandstones adjacent to salt. Detrital apatite and zircon (U-Th)/He systems are low temperature thermochronometers that document the burial, subsequent reheating, and ultimate exhumation age when minerals cooled below specific He-retention temperatures (Wolf et al., 1996; Stockli et al., 2000; Reiners, 2005). Minerals such as apatite and zircon commonly occur in sandstones and can provide bulk cooling ages of a rock when dated. Because of the thermal conductivity differences between salt and sandstones that are adjacent to a salt structure, elevated or suppressed thermal anomalies could influence the thermal history of a sandstone. Apatite and zircon (U-Th)/He dating has proven reliable in providing cooling ages related to exhuming deeply buried crystalline rocks along thrust faults in Laramide arches in the western Cordilleran (Crowley et al., 2002; Ehlers & Farley, 2003; Peyton et al., 2012; Peyton & Carrapa, 2013). This method has also reliably documented cooling ages of rocks exhumed in the footwall of normal fault blocks in the Basin and Range Province in the western United States (Wells et al., 2000; Stockli et al., 2002; Evans et al., 2015). Additionally, detrital apatite and zircon (U-Th)/He methods can reveal provenance, sediment dispersal patterns, erosional characteristics, and pulses of uplift/exhumation related to tectonic and climatic signals (Rahl et al., 2003; Reiners et al., 2005; Stock et al., 2006; Flowers

et al., 2008). The basis for this dating technique rests on the fact that apatite and zircon minerals contain U and Th which follow a decay chain where each nuclide undergoes α-decay to produce ^{4}He daughter nuclides. The decay equation that describes this process is shown in equation 1 (Wolf et al., 1998):

$$^{4}\text{He} = 8^{238}\text{U}(t)\left(e^{\lambda_{238}t} - 1\right) + 7^{235}\text{U}(t)\left(e^{\lambda_{235}t} - 1\right) + 6^{232}\text{Th}(t)\left(e^{\lambda_{232}t} - 1\right) \quad (1)$$

Where U, Th are the amounts present at time (t) and λ is the decay constant. The isotopic decay for this system occurs at a known rate and the age of a mineral can be determined by measuring the amount of parent nuclides ^{238}U, ^{235}U, ^{232}Th and daughter product ^{4}He in a mineral system. He-retention temperatures, also known as the helium partial retention zone (HePRZ), for apatite are 40 - 90˚C (Wolf et al., 1998) and 140 - 200˚C for zircon (Wolfe & Stockli, 2010). Apatite and zircon exposed to temperatures hotter than the HePRZ result in the total loss of radiogenic ^{4}He from the crystal lattice and yield an age of zero. Temperatures within the HePRZ allow some of the ^{4}He daughter product to remain in the crystal lattice with the remainder diffusing out of the crystal (Wolf et al., 1998). Minerals at temperatures below the HePRZ retain all ^{4}He in the crystal lattice and give the age of when the crystal cooled below its closure temperature.

Farley et al. (1996) recognized that (U-Th)/He dating techniques could give erroneously young apatite/zircon-He ages due to the high kinetic energy of alpha decay. When ^{238}U, ^{235}U and ^{232}Th undergo alpha decay, the ^{4}He daughter product is emitted with a characteristic kinetic energy (MeV) capable of ejecting an alpha particle out of the crystal lattice. If the daughter product is retained within the crystal, it travels some distance within the lattice before it comes to rest that is known as the stopping distance (S). The kinetic energy of the alpha particle and the density of the mineral affect the stopping distance. The range of the stopping distance is between ~11 and 34 μm depending on the parent nuclide. Importantly, smaller apatite/zircon

crystals with the shortest diameter < 60 μm are avoided because they lose the majority of ^{4}He due to alpha ejection. Zircon that displays chemical zonation are also avoided. Rims of zoned zircons can be enriched in U and Th near mineral grain boundaries thereby ejecting anomalous amounts of daughter nuclides from the crystal lattice. In addition, apatite crystals with mineral inclusions are avoided because they can introduce excess U and Th into the system. Crystals > 60 μm are also influenced by alpha ejection, but we correct for this phenomenon by following correction procedures outlined by Farley et al. (1996). Using this method, we calculate an (F_T) by measuring the dimensions of an apatite/zircon grain and determining the surface to volume ratio for that crystal. The F_T defined by Farley et al. (1996) is proportional to the surface to volume ratio of a crystal. Thus, a smaller crystal has a larger surface to volume ratio that corresponds to a greater F_T. Conversely, a larger crystal has a smaller surface to volume ratio corresponding to a smaller F_T. A corrected age can be determined from equation 2 (Farley et al., 1996):

$$\text{Corrected Age} = \frac{\text{Measured Age}}{F_T} \quad (2)$$

where a measured age for an apatite/zircon crystal is simply divided by F_T which corrects for any lost ^{4}He due to alpha ejection.

Shuster et al. (2006) demonstrated that apatites with large enough effective uranium concentrations (e[U]) can have significant radiation damage which increases the He retention of an apatite grain. Radiation can cause crystal lattice defects within an apatite thereby enhancing the trapping capability of the mineral and allowing increased amounts of He to accumulate over time (Shuster et al., 2006). Radiation damage can therefore explain anomalously old thermochronologic ages in geologic settings where (U-Th)/He methods should yield young ages.

1.5 Evaluating a Paleothermal Anomaly using Low Temperature Thermochronology

Low temperature thermochronology of detrital apatite and zircon deposited in sedimentary rocks reflect basin scale sedimentary recycling. These mineral systems initially crystallize from a magma chamber in their source region and are subsequently exhumed and cool below their He-retention temperatures. These rocks are then eroded, transported, and deposited in a sedimentary basin where they may be buried by continued deposition. Once buried deeply enough, detrital apatite/zircon (U-Th)/He mineral systems are reset by increases in temperature from burial. These rocks can be exhumed again by renewed tectonic/erosional processes and undergo cooling. During cooling, subsurface isotherms shift downward and temperatures are based on the amount of overburden and the geothermal gradient. Figure 5 (Ehler & Farley, 2003) shows the cooling history of a rock as it passes through different isotherms while being exhumed in the footwall of a normal fault block. Dating an exhumed sandstone sample collected from the surface provides the age when the rock cooled below its HePRZ while passing through isotherms provided that it was buried deeply enough to be completely annealed.

One of my goals was to use apatite and zircon (U-Th)/He dating to determine the most recent cooling history of sandstones that lie adjacent to a salt structure. Sandstones near the top of a salt structure are predicted to be exposed to an elevated temperature anomaly and correspondingly have a different temperature history than sandstones farther away from a salt structure. Sandstones farther away from salt are predicted to be exposed to cooler temperatures because they are beyond the influence of heat flow associated with salt. Consequently, sandstones at higher temperatures take longer to cool below their He-retention temperature zone which should produce younger apatite/zircon He-ages. Sandstones in supra salt positions that are farther from a salt structure are at cooler temperatures and should pass through their He-retention

temperature zone, assuming they were buried deeply enough to reset them, before near salt sandstones giving an older apatite/zircon He-age. Sandstones farther from salt may also retain their original exhumation age if they are not exposed to elevated temperatures. As such, an age trend of younger apatite/zircon He-ages are predicted to occur near a salt structure while ages of sandstones should be older with increasing distance away from a salt structure (Fig 6). This dating method in addition to an analysis of silica cement in sandstones could perhaps test whether or not a paleothermal anomaly is present in sandstones adjacent to a salt structure. Together these methods may reveal the extent and scale of a paleothermal anomaly and characterize the interaction between an elevated thermal anomaly associated with a salt structure and adjacent sandstones.

1.6 Hypothesis

Numerical simulations predict that symmetrical elevated thermal anomalies exist at the top of salt structures and extend ~ 1–1.5 times the radius of a salt structure into adjacent strata. The goal of this work was to test for the presence of a paleothermal anomaly in exposed strata adjacent to a salt wall to field test predictions made by numerical models. It is hypothesized that an elevated thermal anomaly existed at the top of salt structure and extended into adjacent stratigraphy in the geologic past. It is predicted that this paleothermal anomaly influenced the thermal history of strata adjacent to the salt structure and can be detected by low-temperature thermochronology and a silica cement analysis. The results of this work improve our evolving understanding of salt thermal anomalies and ground truth the predictions made by numerical models.

CHAPTER 2: GEOLOGIC SETTING OF FIELD AREA

2.1 Field Area Location

To test the hypotheses, a field area within the Paradox basin was selected which contains some of the best exposed salt structures in North America and serves as a well-studied natural laboratory for testing hypotheses related to salt. The Paradox basin is located within the Colorado Plateau in southeastern Utah and southwestern Colorado. The basin is a large sedimentary assemblage marked by numerous salt cored anticlines and salt walls that trend parallel to the Uncompaghre uplift (Fig. 7) (Lawton and Buck, 2006). The salt walls and associated anticlines occur as NW-SE trending elongated valleys created by salt collapse from dissolution (Hudec, 1995). The Onion Creek salt wall in Fisher Valley (Fig. 10) was selected for this research because the salt wall is well exposed at the surface and lies adjacent to easily accessible sandstones of the Cutler Group.

2.2 The Paradox Basin

During the Early Pennsylvanian, the Ancestral Rocky Mountain orogeny produced a series of thick-skinned thrusts in present-day North America as a result of northwest directed flat slab subduction during the convergence of present day North America and South America (Ye et al., 1996; Barbeau, 2003). The Paradox basin was subsequently created when the southwest-verging Uncompaghre thrust fault initiated as part of the Ancestral Rocky Mountain orogeny. The Uncompahgre thrust fault carried Precambrian crystalline rocks and Cambrian through Devonian strata in the hanging wall of the uplift (Ohlen & McInyre, 1965; Barbeau, 2003). Loading of the crust by the Uncompaghre uplift produced an intraforeland flexural basin to the southwest (Barbeau, 2003).

The Uncompaghre uplift induced downflexural folding which created accommodation for sediment accumulation within the newly formed basin. During the Pennsylvanian, repeated incursions of a restricted, shallow marine sea deposited a thick succession of evaporates consisting of halite, anhydrite, and other salts (~2,500 m thick) with minor amounts of limestone, shale, and sandstone representing the Hermosa Group including the Paradox Formation (Fig. 9) (Ohlen & McInyre, 1965; Nuccio & Condon, 1996; Trudgill, 2011). The cyclical deposition of evaporates is thought to represent the repeated flooding and retreat of sea level into and out of the Paradox Basin in response to glaciation during the Pennsylvanian (Hite & Buckner, 1981). The Late Pennsylvanian Honaker Trail Formation rests above the Hermosa Group and represents a shallow marine near shore depositional environment. In the Late Pennsylvanian and Early Permian, sediments derived from the highlands of the Uncompahgre uplift were eroded and transported into the basin. These sediments became the Cutler Group and are composed of arkosic fluvial sandstones interbedded with very minor amounts of eolian sandstone near the Uncompahgre uplift (Langford & Chan, 1988). Proximal Cutler Group sandstones represent alluvial fans with braided fluvial channel systems within the foredeep of the Paradox Basin (Condon, 1997; Barbeau, 2003). More distal parts of the Cutler Group contain increased occurrences of eolian sandstones that prograde southwestward and interfinger into the marine/eolian Cedar Mesa Formation SW of the basin back-bulge (Langford & Chan, 1988). Overall, well-log data indicate that the Cutler Group largely fines upward. Lower section paleocurrent data show SW-W flow direction while the upper Cutler shows N-NE paleocurrents (Trudgill, 2011).

2.3 Onion Creek Salt Wall Growth, Depletion, and Collapse

As the Uncompahgre uplift shed sediments into the basin during the Late Pennsylvanian and Early Permian, loading of the Honaker Trail Formation and the later Cutler Group atop the salts of the Paradox Formation, coupled with normal faulting, initiated salt movement (Vendeville & Jackson, 1992a; Hudec, 1995; Kluth & Duchene, 2009). Salt wall anticlines in the Paradox basin are situated over normal fault basement steps, which are thought to control the location and, in part, initiation of salt wall growth (Hudec, 1995; Doelling, 2002). However, Trudgill (2011) suggested that these basement normal faults accommodated flexure of the crust due to continued movement along the Uncompaghre Fault rather than being a result of regional extension. In any case, continued salt movement was a result of passive diapirism (Trudgill, 2011) as defined by Rowan (2003) where growth of a salt body at or near the surface of the Earth is due to sediment loading on a salt source layer. Salt walls in the Paradox basin grew in a NW-SE orientation during active Cutler progradational deposition that increased overburden on the source layer of salt causing it to evacuate into the salt wall position (Hudec, 1995; Kluth & Duchene, 2009; Trudgill, 2011). Local thinning of growth strata onto the flanks of the Onion Creek salt wall supports active salt rise throughout the Permian (Fig. 10) (Trudgill, 2011). If sediment accumulation rates outpace salt evacuation, then salt will become depleted at the source layer and a horizontal salt weld will form creating an unconformable contact between rocks above and below the preexisting horizontal salt layer (Rowan, 2003). In the case of Onion Creek, the salt source layer became depleted during the Triassic and formed a salt weld in its present day configuration (Fig. 10) (Trudgill, 2011). Jurassic age sediments were later deposited during a time of no active salt movement because the salt source layer had become depleted along with the formation of salt welds. Cretaceous age rocks are not present in the immediate

area however they do occur roughly 10 km to the northeast and along the margins of the Paradox basin (Condon & Nuccio, 1996; Doelling and Ross, 1998; Doelling, 2002; Trudgill, 2011). Cretaceous and Tertiary sediments once buried the Onion Creek salt wall in the form of a salt cored anticline (Condon & Nuccio, 1996; Doelling, 2002). In the Permian, the crest of the Onion Creek salt was elevated with respect to the surrounding terrain. Later deposition of Triassic and Jurassic sediments then capped the salt wall producing a salt cored anticline. Moreover, the collapse of Permian – Jurassic stratigraphy into the Onion Creek salt wall (Fig. 10) is thought to have occurred from the Late Tertiary through Quaternary as a result of erosion and salt dissolution (Doelling, 2002). The present day width of the upper part of the Onion Creek salt wall at or near the surface is roughly 2.7 km (Doelling, 2002). Lastly, the northern side of the salt wall unconformably contacts the Cutler Group at the surface (Fig. 10).

2.4 Previous Estimates of Stratigraphic Thicknesses and Paleotemperatures at Onion Creek

It is important to estimate paleotemperatures at the top of the Cutler Group at Onion Creek to determine whether or not these sandstones became hot enough to reset detrital apatite/zircon-He systems. Condon & Nuccio (1996) evaluated the burial and thermal history of organic rich shales interbedded with Paradox Formation salt cycles to determine the hydrocarbon potential of the Paradox Basin. They created a burial, thermal, and petroleum generation model for this area near Moab, UT which lies 7 km southwest of the Onion Creek salt wall (Fig. 10). They report that the top of the Permian Cutler Group reached a maximum temperature of >200˚F (93.3˚C) near Moab, UT. Their subsidence and thermal models were generated from a combination of source rock characterization techniques including Rock-Eval pyrolysis analysis, vitrinite reflectance (R_o), and estimating stratigraphic thicknesses from 200 geophysically

correlated well logs. Source rock potential characterization allows for determination of thermal maturation that correlates to a maximum exposure temperature that a rock may have been exposed too. Estimating stratigraphic thickness also provides further constraints on temperature by examining how subsurface isotherms are affected by different degrees of burial. The modeled temperature estimate of 93.3˚C provides a first order glimpse at a potential temperature estimate of the top of the Cutler Group at Onion Creek, UT.

CHAPTER 3: METHODOLOGY

3.1 Sample Collection

Nine sandstone samples were collected from the Cutler Group along a north-trending transect perpendicular to the Onion Creek salt wall (Fig. 12). The transect begins close to the contact between the Cutler Group and the Onion Creek salt wall and extends ~ 4.13 km away from the salt wall. Sample location sites were spaced ~ 500 meters apart. A four km transect was chosen because theoretical calculations predicted that a paleothermal anomaly should extend 1.5 times the width of the 2.7 km wide Onion Creek salt wall. Strike and dip data from Doelling (2002) showed that the Cutler Group dips to the north at about ~ 3.5˚ away from the salt wall. Because of the dip of the strata, samples taken from the Cutler Group along the transect were not from the same stratigraphic horizon; instead samples were collected from progressively higher stratigraphic levels. We calculated that the perpendicular transect climbs 244 meters upward through the stratigraphy of the Cutler Group which equates to a decrease in temperature of 7.3˚C assuming a normal geothermal gradient (25˚C/km) (Fig. 13). A decrease in temperature of 7.3˚C from the beginning to the end of the transect is a small temperature bias when considering the range of He-retention temperatures for apatite (40 - 90˚C) and zircon (140 - 200˚C).

Sample location sites were first targeted using satellite and topographic maps according to 500 meter spacing but were later adjusted based on accessibility in the field. Sample sites were selected in the field based on outcrops that had less weathering. An attempt was made to take samples from the lowest possible stratigraphic horizon. Fine-grained sandstones were chosen for consistency and the first few centimeters of weathered rock were removed before breaking off samples with a sledge hammer. After removal from the outcrop, individual samples were broken into smaller pieces and placed into three separate plastic bags, duct taped closed,

labeled, and placed into a cloth sample bag to avoid cross contamination. Latitude and longitude coordinates and elevation were recorded using a handheld GPS device at each sample location. In addition, each sample was given a Pettijohn sandstone classification name (Pettijohn, 1975) along with a grain size determination in the field.

3.2 Thin Section Preparation and Point Count Procedure

A small billet was cut from each sample collected along the perpendicular transect. Billets were sent to Quality Thin Sections in Phoenix, USA for thin section preparation. All billets were impregnated with a blue epoxy to highlight pore spaces in sandstone thin sections. Five hundred point counts were conducted on each thin section using a 50x binocular petrographic microscope. Each thin section was placed into a point counting mechanism that was attached to the stage of the microscope which shifted an incremental space after each point count. Point counts were recorded into a mechanical counter and then transferred to an Excel spreadsheet. Each point count was conducted at 10x magnification to maintain consistency. Thin section samples with grain sizes less than that of very fine sand (< 63 μm) were omitted from point counting because these are mudrock. Eight different components of the sandstone were point counted: framework grains, pore space, intragranular pore space, matrix, carbonate cement, silica cement, dolomite cement, and unknown. Thin section sample numbers were also hidden during point counts to minimize user bias.

3.3 (U-Th)/He Preparation and Isotopic Measurements

Whole samples were fed through a jaw crusher and then a disk mill to produce medium/fine sands. Both machines were taken apart and thoroughly cleaned between running samples to avoid cross contamination. Samples were then sent to GeoSep Services to separate

apatite and zircon from crushed sands by sieving, heavy liquid and magnetic separation outlined by Donelick et al. (2005).

Apatite/zircon crystal selection and isotopic dating took place at the Noble Gas Geochronology and Geochemistry Laboratories (NG^3L) at Arizona State University. A Leica MZ16 binocular microscope was used to select apatite/zircon crystals that were larger than 50 μm in the minimum dimension. Three crystals and two spares were selected for He-dating for each sample. An aliquot of apatite crystals were selected based on the following criteria: (1) euhedral hexagonal morphology, (2) free of mineral/fluid inclusions, and (3) homogenous crystal sizes. All selected detrital apatites were highly abraided with well-rounded terminations due to high degrees of transport and weathering. In cases where samples lacked apatite crystals with two terminations, an aliquot of apatites were selected based on having similarly broken terminations to maintain consistency. Apatite crystals were measured for surface/volume ratio determinations for the alpha ejection correction factor (F_T) following Farley et al. (1996) (Fig. 14a). Likewise, zircon crystals were selected based on the following criteria: (1) euhedral tetragonal morphology, (2) homogenous crystal sizes, (3) no chemical zonation, and (4) no apparent radiation damage. Unfortunately, four samples lacked an abundance of zircons with a minimum dimension of > 50 μm. In samples 15RN06, 15RN07, 15RN10, and 15RN12 one selected zircon from each sample had a minimum dimension of ~ 45 μm. Each selected zircon was measured for F_t determinations following the procedure described by Hourigan et al. (2005) (Fig. 14b). While each apatite/zircon grain was being measured, crystals were simultaneously photographed with a digital video camera attached to the binocular microscope. After measurements for each crystal were made, samples were loaded into a Niobium tube, clamped shut on each end, and placed into a labeled vial. Isotopic $^4He/^3He$ ratios were measured using an

Alphachron MkII mass spectrometer built by CSIRO/Patterson Instruments/ASI. He-gas from the sample was extracted by heating a loaded mineral grain with a 970 nm diode laser and subsequently spiked with a ^{3}He standard. Extracted sample gas and the ^{3}He standard were then accelerated down the flight tube and measured by the mass spectrometer. After measuring the He-isotopic ratios, each crystal was dissolved at high temperature and pressure in 25 μl of 50% nitric acid, diluted with a U-Th standard, and then placed into Thermo Scientific ICAP Q inductively coupled plasma mass spectrometer to measure U-Th isotopic ratios. For a more complete procedural review of (U-Th)/He dating techniques at Arizona State University's NG^{3}L laboratory see van Soest et al. (2011).

CHAPTER 4: RESULTS

4.1 Estimates of Stratigraphic Thickness and Paleotemperatures

Unpublished vitrinite reflectance data (Personal Communication, Hanson, 2016) report Ro values of ~ 0.75 (~ 80˚C) for the Tunnock Member of the Mancos Shale (Lower Cretaceous) to the northwest approximately 45 km from the Onion Creek salt wall. Assuming Cretaceous rocks were once present at Onion Creek we can estimate hypothetical paleotemperatures of the subsurface before erosion took place. The top of the Permian Cutler Group was once capped by 580 meters of Jurassic and Triassic sedimentary rocks (Doelling and Ross, 1998) which corresponds to 17.4˚C in a normal geothermal gradient (25˚C/km). Adding together the thermal maturation temperature of nearby Cretaceous rocks corresponding to 80˚C and the temperature from thicknesses of both Jurassic and Triassic rocks (17.4˚C) suggests the top of the Permian Cutler Group may have reached a temperature of 97˚C due to burial depth alone. This temperature is high enough to induce silica cementation, thought to occur beginning at 80˚C and is also high enough to completely reset detrital apatite for (U-Th)/He dating. Unfortunately, this temperature estimate is too low to reset detrital zircon. Overall, the 97˚C temperature estimate expresses a paleotemperature at the top of the Cutler Group assuming the accuracy of extrapolated Ro values of Cretaceous rocks and a normal geothermal gradient.

4.2 Silica Cementation Analysis

All twelve sandstone samples were classified as feldspathic litharenites in the field and represent braided fluvial channel systems with largely immature but highly abraded sands. Point counted thin section samples range from very fine (124 μm) to medium (500 μm) grained sands and consist mostly of fractured angular quartz with lesser amounts of plagioclase, biotite,

muscovite, and microcline (Fig. 15). Samples 15RN02, 15RN09, 15RN10, and 15RN11 have grain sizes of less than 63 μm constituting these samples as mudrocks which could not be point counted for a silica cement analysis. The results from point counts are summarized in Table 1. A total of 15 silica cements were observed in thin section from all of the samples together and constitute the minority of cements. The majority of cements within the sandstones are carbonate cements, which have no implications for determining paleotemperatures as calcite cement can precipitate over a range of temperatures (Fig. 16). Figure 17 shows no clear relationship between any of the point counted parameters with respect to increasing/decreasing distance from the Onion Creek salt wall. There is an inverse correlation between carbonate cements and pore space (Fig. 17).

4.3 Apatite-He Ages and Uncertainties

Weighted mean apatite-He ages and associated two standard deviation weighted mean uncertainties are shown in Table 2 and range from 17.9 ± 3.5 Ma to 33.5 ± 0.8 Ma (Early Oligocene – Early Miocene). Isotopic measurements and raw apatite-He ages are reported in Table 4. Apatite-He ages are plotted versus distance from the Onion Creek salt wall in Figure 18. A regression line was fit to the data without incorporation of uncertainties and no correlation between distance from salt wall and (U-Th/He) age was found. Nonetheless, the large uncertainties associated with the ages of samples 15RN05, 15RN06, 15RN08, and 15RN09 mask the detection of any discernable age trend. Large reported uncertainties are the result of over dispersed (U-Th)/He age populations. Three raw ages are calculated for each sample aliquot and an aliquot's dispersion is assessed using a mean squared weighted deviation (MSWD). The MSWD was used to assess how well an age calculation regression line fit to our empirical isotopic data (Wendt & Carl, 1990). An acceptable MSWD was calculated for each age based on

the number of sample points and degrees of freedom (2) and then a true MSWD was determined for each weighted mean age. If the MSWD exceeded calculated acceptable values, then an aliquot is over dispersed and requires an error expansion where the analytical two standard deviation uncertainty was multiplied by the square root of the MSWD (Evans, 2015).

The Hampel Identifier method was also used to determine outliers in over dispersed age aliquots recognized by the MSWD. The Hampel method is a robust statistical test uniquely sensitive to outliers because it uses the median rather than the mean to calculate the absolute deviation from the central most value to quantify ages that fall outside of acceptable limits (Hampel, 1971). For apatite, outlier ages are commonly the result of unrecognized mineral inclusions bearing excess parent and daughter material which can be difficult to detect optically.

4.4 Zircon-He Ages

Weighted mean zircon-He ages and associated two standard deviation weighted mean errors are reported in Table 3 and range from 721 ± 15 Ma to 204 ± 147 Ma (Middle Neoproterozoic – Late Triassic). Isotopic ages and raw zircon-He ages are reported in Table 5. Zircon-He ages are plotted versus distance from the Onion Creek salt wall in Figure 19. A linear regression was fit to the data without incorporating uncertainties and a moderate negative correlation (R = - 0.67) was found between zircon-He ages and distance from the salt wall (Fig. 19). However, sample 15RN12 shows highly dispersed ages and a large calculated mean squared weighted deviation (Tables 3 and 5). Thus, the weighted mean age for sample 15RN12 is unreliable because of the large statistical dispersion and replotting the zircon-He age versus distance from salt shows little evidence for any age trend (Fig. 20). Based on the data, we detect no correlation between age trends and distance from salt. No weighted mean age is reported for sample 15RN08 because the ages within the aliquot are highly over dispersed (Tables 3 and 5).

CHAPTER 5: DISCUSSION

5.1 Silica Cements and Porosity

My point count analysis provides no insight into paleotemperatures in the Cutler Group adjacent to the Onion Creek salt wall due to the lack of silica cementation. The Cutler Group is composed of highly texturally immature sands that are poorly sorted. The textural immaturity and relative abundance of clay matrix material suggests that the Cutler Group had a low initial porosity and permeability. Low initial permeability impedes pore fluid flow and without abundant pore space little room exists to precipitate cements. While calcite cements do occur in the Cutler Group their presence indicates that what little pore space was available after deposition was cemented by calcite. Calcite cements can form at either low or high temperatures thus their presence does not indicate the temperature of or timing of cement formation. These processes would have restricted the flow of pore fluid water and made it difficult for the later precipitation of other cement types.

5.2 Lack of a Thermal Anomaly and Thermohaline Pore Fluid Convection

No definitive evidence exists for an apatite/zircon-He age trend with respect to distance from the Onion Creek salt wall and the hypothesis that an elevated paleothermal anomaly exists in the Cutler Group cannot be supported. We hypothesized that an elevated thermal anomaly existed because numerical models (Selig & Wallick, 1966; Jensen, 1983; Petersen & Lerche, 1995; Nagihara, 2003), well temperature measurements from drilled salt diapirs (Vizgirda et al., 1985; Yu et al., 1992), and a field study (Hanson, 2014) found evidence for elevated thermal anomalies near salt crests. Numerical simulations predict that a thermal anomaly would extend 1.5 times the radius of a salt structure into adjacent sedimentary rocks and could elevate

temperatures by as much as 30˚C. If an elevated thermal anomaly existed, our data should record an anomaly within the Cutler Group assuming we have accounted for all of the geologic processes that influence temperature.

Models assume a number of geologic simplifications to reduce the overall complexity of numerical simulations. Simulations often utilize basic salt geometries (salt blocks, vertical walls) that are unrealistic in a geologic sense. Salt geometries are commonly highly complex and very rarely form flat vertical/horizontal surfaces. Strata adjacent to salt structures are largely modeled as thick sequences of homogenous rock types. Near-salt stratigraphy is often interbedded with various rock types which would create numerous thermal conductivity interfaces adjacent to salt. Therefore modeling a single thermal conductivity contrast between strata adjacent to a salt wall does not accurately portray differences in stratigraphy. Pure halite (NaCl) is also modeled as the sole mineral within salt structures. In reality, a plethora of different halides (sylvite, gypsum, anhydrite, etc.) make up salt bodies in addition to sequences of cohesive stratigraphy (shales, carbonates, sandstones) rafted along with migrating salt. At Onion Creek, an Exxon well was drilled near our perpendicular transect into the Paradox Formation and reports that halite makes up 55.5% of the lithology (Trudgill, 2011). In addition, sandstone, limestone, and shale cycles were also observed in Paradox Formation well logs. Thus, the Onion Creek salt wall is not pure halite but rather 'dirty' salt. With roughly half of the Paradox Formation consisting of pure halite the overall thermal conductivity contrast between the salt wall and Cutler Group should be less significant. Lastly, earlier salt thermal anomaly numerical models neglect to incorporate the thermohaline convection of pore fluids in strata adjacent to salt structures. Geochemical evidence for convecting cells of pore fluids in strata adjacent to salt diapirs within the Gulf of Mexico has been reported (Hanor and Workman, 1986;

Hanor, 1987, Leger, 1988; Jensenius and Munksgaard, 1988). With the recognition of thermohaline convection near salt diapirs, attempts were made to simulate the effect of convecting pore fluids on temperatures in strata adjacent to salt which was distinctly different than earlier salt thermal anomaly numerical modeling (Evans et al., 1989; Griffin, 1989; Evans et al., 1991; Ranganathan, 1992). Heat conduction by salt is thought to primarily initiate convection of heterogeneously saline pore fluids. The combined effect of both temperature and salinity differences create density variations that drive upward ascending columns of hot water through pore spaces near salt that cool and descend. Research performed by Hanor (1987) showed that near salt thermohaline convection can occur on a kilometer scale into adjacent strata. Thus, pore fluid convection driven by a conduction of heat from a salt structure could explain why we see no evidence for a thermochronologic age trend with respect to distance from the Onion Creek salt wall. Convection of hot pore fluids within the Cutler Group may have homogenized the overall temperature of the sandstones which would account for the absence of a prominent (U-Th)/He age trend and mask any thermal anomaly that may have existed (Fig. 22). For further temperature modeling around salt structures, our data suggest that incorporating fluid flow in salt adjacent rocks will enable better temperature estimates and more precise understanding of subsurface isotherm patterns.

Both concepts of ‘dirty’ salt reducing the overall thermal conductivity at Onion Creek and thermohaline pore fluid convection are equally reasonable explanations for the absence of a paleothermal anomaly within the Cutler Group. Abundant geochemical and modeling evidence exists to support thermohaline pore fluid convection. However, we are unaware of any studies that have considered modeling ‘dirty’ salt and a subsequently lower thermal conductivity contrast between salt/strata interfaces. Future work may take these interpretations and test how

different degrees of internal salt compositions might influence the extent and magnitude of a thermal anomaly into adjacent sedimentary rocks.

Lastly, models predict that elevated isotherms exist in strata adjacent to salt within the uppermost ~ 800 meters of a salt wall (Mello et al., 1995). Sedimentary rocks in positions greater than 800 meters below the crest of a salt wall may be outside the influence of an elevated thermal anomaly. At Onion Creek, the sampling transect is somewhere within the uppermost 1000 meters of the salt wall. Because of the uncertainties associated with calculating the exact position of the top of the salt wall before its collapse, we cannot report if the absence of a paleothermal anomaly is a result of the sampling transect being outside of the influence of an elevated thermal anomaly. While we find no evidence for a paleothermal anomaly, models that predict elevated temperatures at salt crests may still be correct given that one considers rocks at the correct position adjacent to a salt wall.

5.3 Apatite/Zircon-He Age Dispersion and Fluid Flow

Weighted mean apatite/zircon-He ages with large uncertainties are the result of over dispersed age populations and weighted mean zircon-He ages for samples 15RN08 and 15RN12 were omitted from the final analysis as a result. Weighted mean apatite-He ages for samples 15RN05, 15RN06, 15RN08, and 15RN09 were dispersed to a lesser degree and kept within the final analysis. The dispersion of ages from these sample locations could be explained by local variations in thermohaline pore fluid convection or be the result of fluid flow along unmapped faults near sample location sites. Such geological processes could cause enough temperature variation to reset or partially reset at least some detrital zircons in these sandstones. At these sample sites, we did not find evidence for hydrothermal alteration in the field, but more detailed

analyses could be performed to confirm the existence of focused zones of heat associated with pore fluids.

Another explanation for age dispersion may reside by fluid interaction with apatite/zircon mineral grains potentially inducing open system behavior. In U/Pb systems, interactions with fluids can create preferential Pb loss which can alter U/Pb ages and this too may affect (U-Th)/He thermochronology. Any process that alters parent or daughter products within a mineral grain can change nuclide ratios thereby giving erroneous ages.

5.4 Apatite-He Ages & Oligocene – Early Miocene Exhumation

We interpret the reported apatite-He ages as being fully reset because their Early Oligocene – Early Miocene ages are markedly younger than the Precambrian basement source terrane of the Uncompahgre Uplift (1.4 - 1.75 Ga) (Hedge et al., 1968; Hansen and Peterman, 1968). These ages reflect the post depositional heating (> 90˚C) within the Cutler Group that fully annealed the apatite mineral system. These ages, coupled with our burial depth estimates help us to reconstruct the subsurface temperature regime of rocks adjacent to the Onion Creek salt wall at a time of maximum burial (Fig. 21). Our sampling transect within the Cutler Group suggests that temperatures exceeded the 90˚C apatite-He partial retention zone. We conclude that apatite-He ages represent local exhumation within the Cutler Group from 17.9 ± 3.5 Ma to 33.5 ± 0.8 Ma. However, many workers report regional exhumation ages of < 10 Ma due to unroofing of the central Colorado Plateau where the Onion Creek field area is located (McMillan, 2006; Pederson et al., 2007; Hoffman, 2009; Cather et al., 2012; Roberts et al., 2012; Evans, 2016). Our sampling transect within the Cutler group lies in close proximity (~ 15 km) to the La Sal igneous intrusion with reported crystallization ages of 25 Ma (Stern et al., 1965) and 20 – 30 Ma (Sullivan et al., 1991). Apatite fission track ages from La Sal igneous rocks range

from 27 – 33 Ma and lie roughly 15 km from our sampling transect at Onion Creek (Chew & Donelick, 2012; Ronnevik et al., 2014). La Sal crystallization ages and apatite fission track ages match remarkably well with our reported apatite-He ages within the Cutler Group. We conclude that the emplacement of the La Sal laccolith into the crust uplifted nearby Mesozoic and Cenozoic stratigraphy thereby increasing erosional rates which cooled detrital apatites in the Cutler Group below their He-retention temperatures during the Middle – Late Oligocene. The Henry Mountains are made up of multiple Oligocene laccoliths and the system is roughly analogous to the La Sal range in terms of age and style of igneous emplacement. The Henry Mountains (145 km southwest of the La Sal) provide an excellent example of folding and uplift Cenozoic/Mesozoic sedimentary overburden in response to laccolith emplacement (Jackson, 1998). The Cutler Group is present at the Henry Mountains and is folded and uplifted due to laccolith emplacement. Apatite-He ages reflecting exhumation of sedimentary overburden associated with laccolith uplift was reported in the Henry Mountains, Utah (Murray et al., 2011). Our results support that laccolith uplift can in fact influence cooling histories of sedimentary overburden and may explain our uniquely old apatite-He cooling ages within the central Colorado Plateau.

5.5 Zircon-He Ages & Proposed Neoproterozoic Exhumation

Based on our burial reconstruction plus largely Neoproterozoic zircon-He ages, we conclude that paleotemperatures in the Cutler Group were not high enough to reset or partially reset the zircon (U-Th)/He mineral system (Fig. 21). Thus, zircons within Cutler Group sandstones record a Neoproterozoic exhumational cooling signal while they resided in the Uncompahgre basement. The Cutler Group has a well-established provenance sourced from the basement of the once uplifted Uncompahgre highlands (Mack, 1977; Mack & Rasmussen, 1984;

Condon, 1997; Barbeau, 2003). This line of evidence, in addition to the lack of any known Neoproterozoic age basement in North America supports that detrital zircon within the Cutler Group is sourced from the Uncompahgre uplift. Crystallization ages of the Uncompahgre basement from high temperature U-Pb and Rb-Sr systems range from 1.4 – 1.75 Ga (Hedge et al., 1968; Hansen & Peterman, 1968). Our detrital zircon-He ages support that the basement of the Uncompahgre underwent exhumation and cooling some time during the Neoproterozoic (Late Cryogenian – Early Ediacaran). These ages also support that at least 8 km of overburden, necessary for temperatures > 200˚C to reset zircon-He systems, buried the Uncompahgre basement prior to Neoproterozoic exhumation. During the Neoproterozoic, the breakup of the continent Rodinia is thought to have initiated around 820 – 700 Ma and culminated by ~ 550 – 600 Ma (Yonkee et al., 2014 and references therein). Our reported zircon-He ages may be a result of cooling of the Uncompahgre basement related to rifting of the supercontinent Rodinia during the Neoproterozoic. These ages are significant because few Neoproterozoic rocks are exposed in eastern Utah and these results shed light on the enigmatic geologic history of the Precambrian in North America.

CHAPTER 6: CONCLUSIONS

We report apatite/zircon (U-Th)/He ages and porosity data for nine sandstone samples taken from the Permian Cutler Group to test for a paleothermal anomaly. No definitive evidence exists that supports an apatite/zircon-He age trend with respect to the distance from the Onion Creek salt wall. Similarly, there is no evidence for increases of silica cements in the sandstones, and thus, does not support our hypothesis that an elevated thermal anomaly existed in sandstones adjacent to the Onion Creek salt wall.

Although a number of possible explanations exist for the absence of a thermal anomaly, both thermohaline pore fluid convection and 'dirty' salt compositions are equally reasonable explanations for the lack of a paleothermal anomaly at Onion Creek. Geochemical and physical evidence for recirculation of pore fluids has been observed in rocks adjacent to salt diapirs in the Gulf of Mexico and is not an uncommon occurrence in hydrocarbon exploration. Further work could test the hypothesis that 'dirty' salt might impede the extent and magnitude of a thermal anomaly by reducing the thermal conductivity contrast between salt and adjacent sedimentary rocks.

Reported apatite-He ages show Oligocene to Early Miocene cooling ages within the Cutler Group at Onion Creek. These ages are fully reset because they are much younger than the Uncompahgre source terrane confirming > 90˚C burial temperatures but are significantly older than previously reported apatite-He cooling ages within the central Colorado Plateau (< 10 Ma). Our reported Onion Creek cooling ages are similar to apatite fission track and crystallization ages of the La Sal igneous province suggesting laccolith emplacement of the La Sal uplift exhumed the nearby Cutler Group sandstones roughly ~ 15 km away around ~ 25 Ma. Detrital apatite-He ages in the Cutler Group from the Henry Mountains record uplift of sedimentary

rocks by emplacement of an igneous intrusion. The Oligocene Henry Mountain igneous intrusion is analogous in timing and style of emplacement to the La Sal which supports that laccolith igneous intrusions can uplift sedimentary overburden resulting in cooling.

Our reported zircon-He ages are Neoproterozoic and suggest that temperatures within the Cutler Group remained below 200˚C and that burial temperatures did not influence zircon (U-Th)/He mineral systems. The largely Neoproterozoic zircon-He ages are younger than the crystallization age of the Uncompahgre basement (1.4 – 1.75 Ga) which supports an exhumation event during the Neoproterozoic at this location in eastern Utah. These ages also reflect post exhumational burial amounts of ≥ 8 km of overburden which are required to provide high enough temperatures (200˚C) to reset zircon-He mineral systems. During the Neoproterozoic, present day central Utah underwent rifting during the breakup of the supercontinent Rodinia. Our reported zircon-He ages may support exhumation related to the rifting of Rodinia in eastern Utah where few to any Neoproterozoic rocks are exposed.

FIGURES

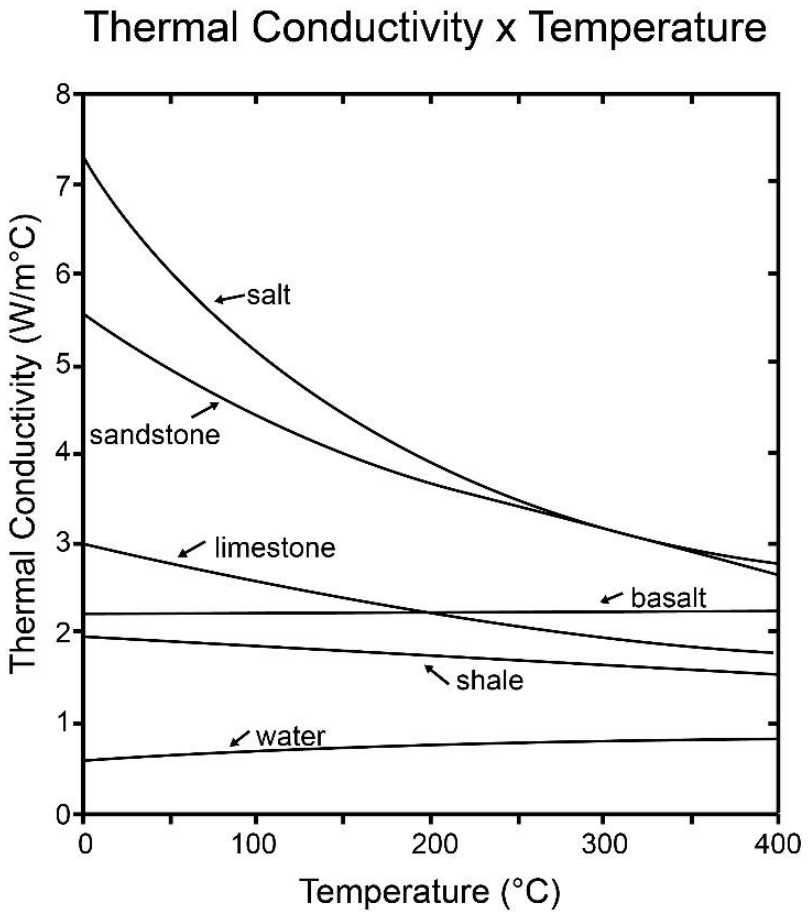

Figure 1. Thermal conductivity of salt versus other rock types. Rock salt in the form of halite has a thermal conductivity of two to four times higher than most other rock types. In addition, the thermal conductivity of rocks typically increase at lower temperatures (Mellow et al., 1995).

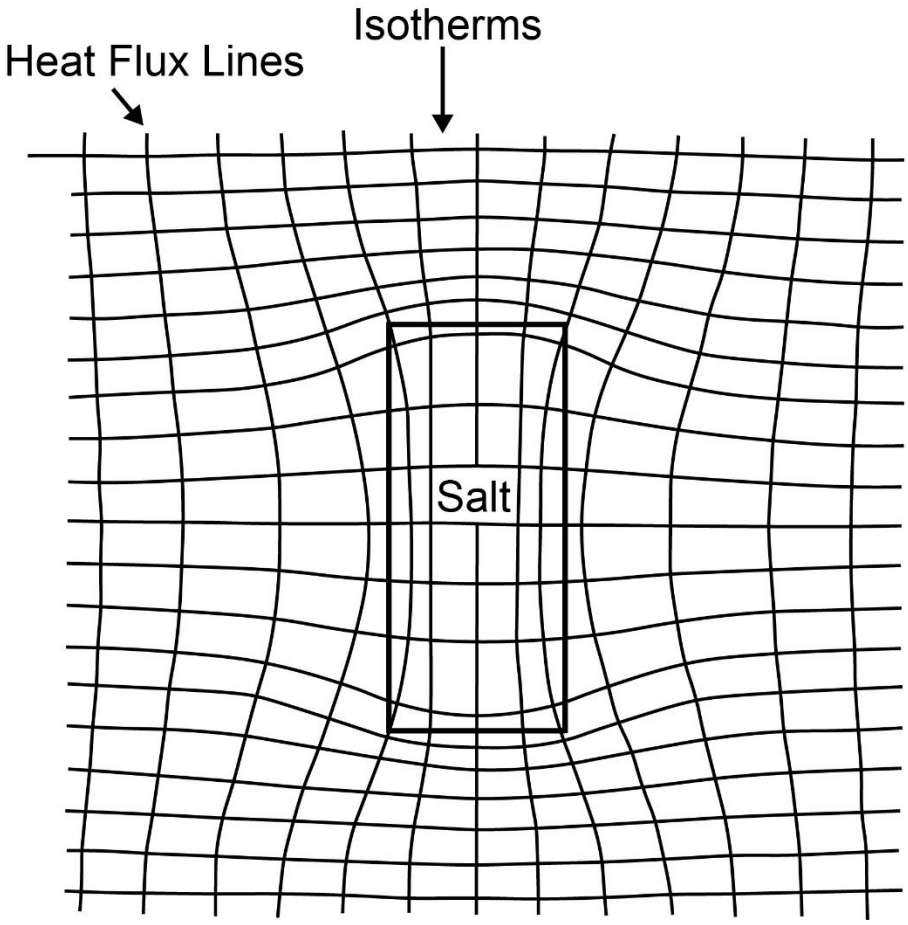

Figure 2. Modelled block of salt in the subsurface showing the distribution of isotherms depicting an elevated and suppressed thermal anomaly at the top and bottom respectively of a salt structure. Isotherms indicate lines of constant temperature (Vizgirda et al., 1985).

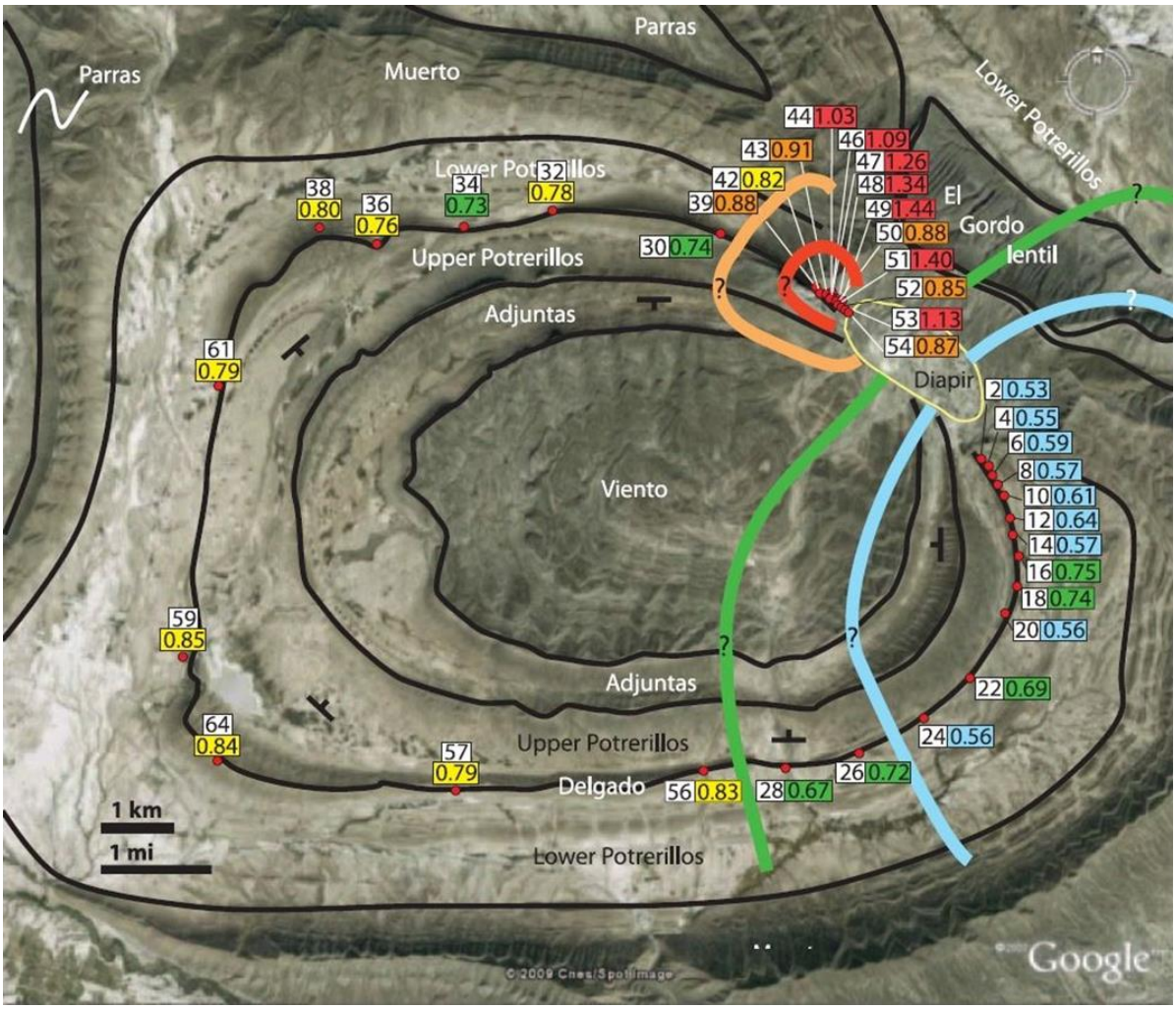

Figure 3. El Gordo diapir (yellow circle) intersects mudstones of the Potrerillos Formation that are visible at the surface of the Earth along the rim of a structural bowl. An elevated paleothermal anomaly (red lines) occurs in mudstones to the northwest of the diapir. A larger suppressed paleothermal anomaly (blue lines) occurs to the southeast of the diapir. High degrees of thermal maturation are indicated by R_o values in red boxes. Lower thermal maturation values are shown in blue. Sample numbers are shown in white boxes (Hanson, 2014).

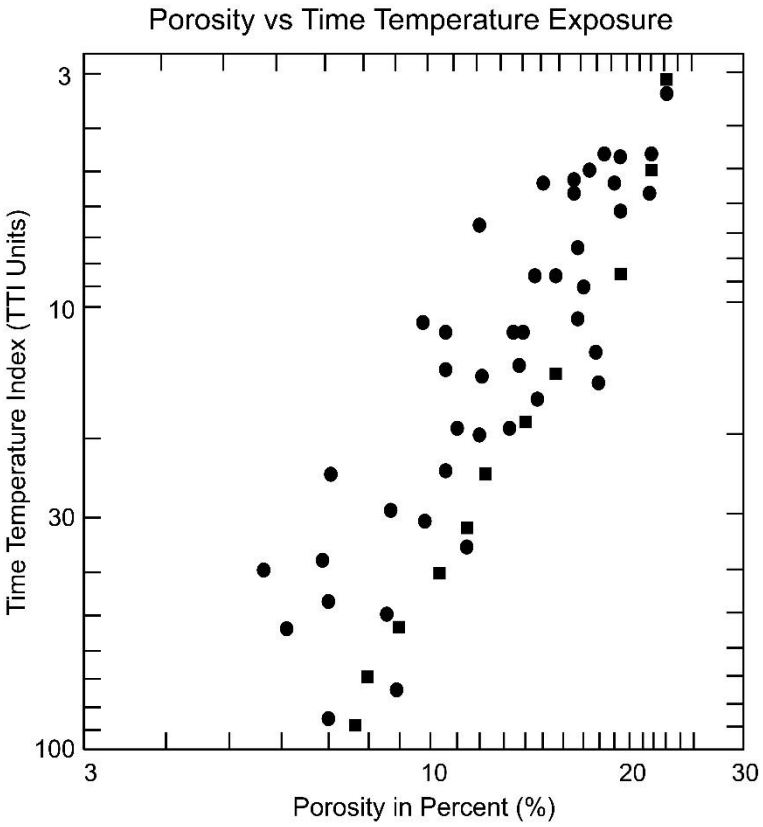

Figure 4. Exposure to elevated temperatures (time temperature exposure) reduce sandstone porosity by initiating quartz cementation. A linear decrease in porosity occurs with increasing exposure to elevated temperatures (Schomoker and Gautier, 1988).

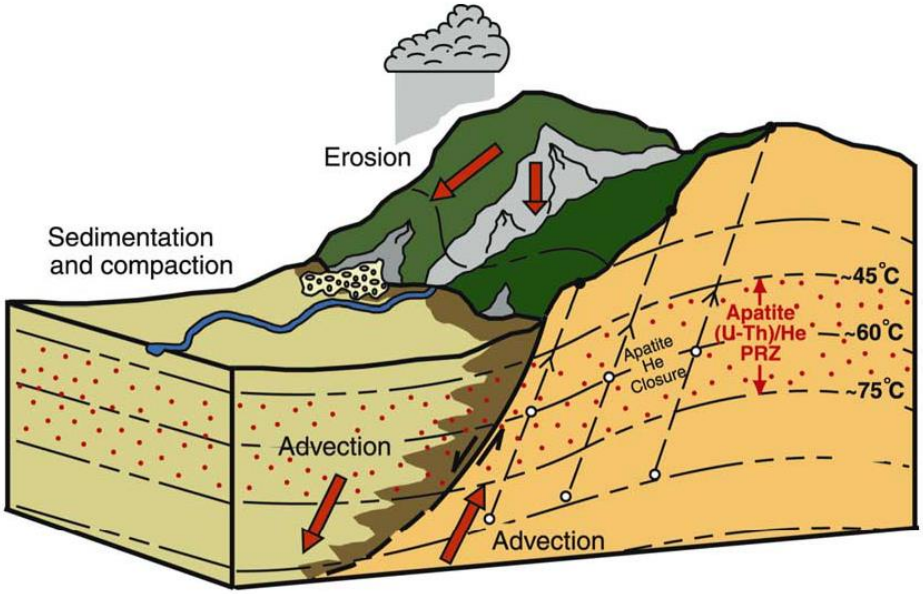

Figure 5. Rocks in the footwall of a normal fault block will cool when exhumed to the surface by passing through isotherms of different temperatures. In other words, isotherms will shift if the amount of overburden is reduced because subsurface temperatures become cooler. This allows rocks to pass through the partial He-retention zone (PRZ) and begin collecting radiogenic ^{4}He (Ehler and Farley, 2002).

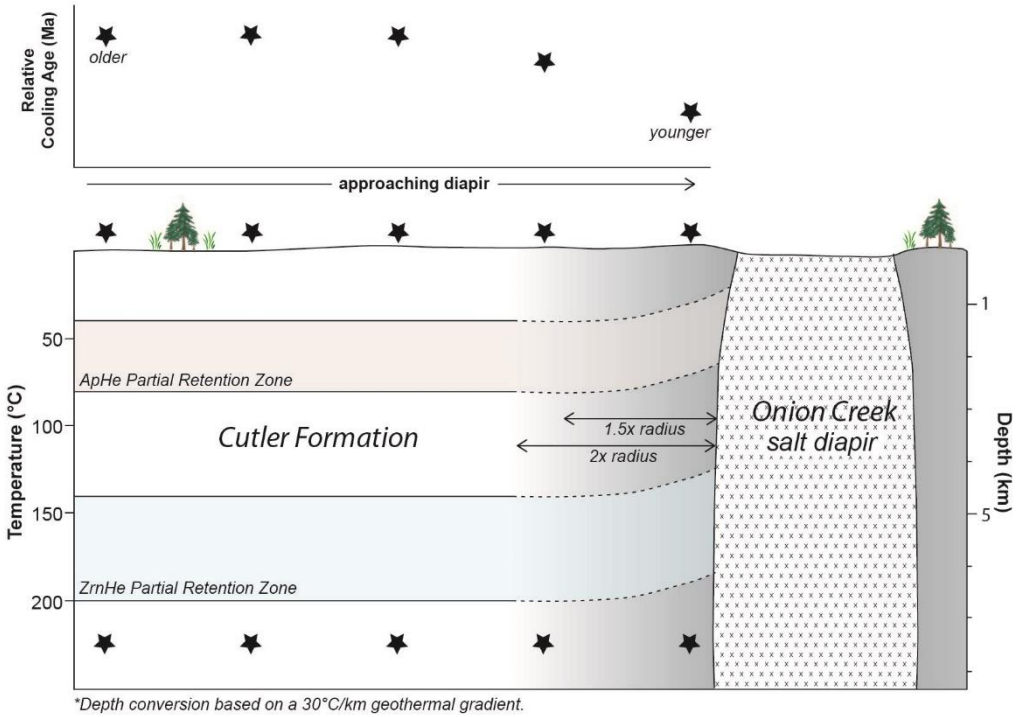

Figure 6. Schematic of an elevated temperature anomaly in Cutler Group sandstones adjacent to the Onion Creek Salt Wall. Sandstones that were once buried at depth and exposed to an elevated temperature anomaly may have a unique cooling history with respect to distance from the diapir. Sandstone sampling locations that have been exhumed by erosion may provide a thermochronologic age trend where ages may become progressively older with increasing distance away from the salt wall. Modified from Evans (2015).

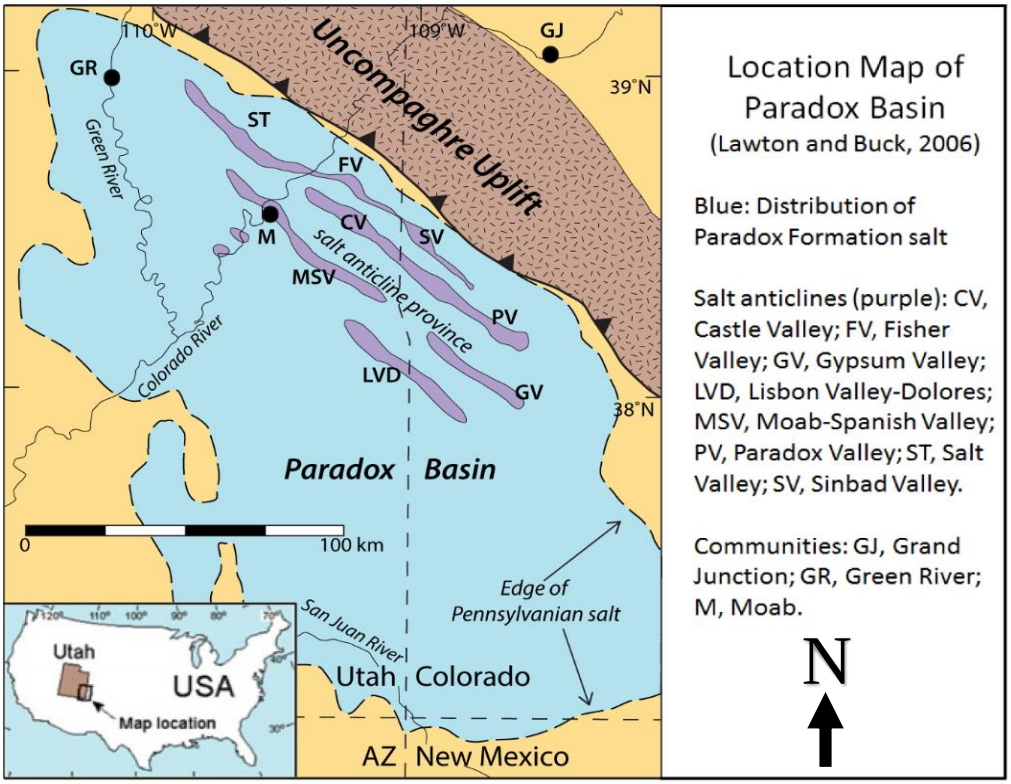

Figure 7. Map showing the location of the Paradox Basin in southeastern Utah and southwestern Colorado. The extent of the basin is controlled by the subsurface occurrence of the Paradox Formation, which consists of a thick sequence of Pennsylvanian age evaporites (blue). Collapsed salt-cored anticlines are the only expressions of salt at the surface (purple). The field area for this study is at Onion Creek, UT near the Fisher Valley (FV) salt anticline (Lawton and Buck, 2006).

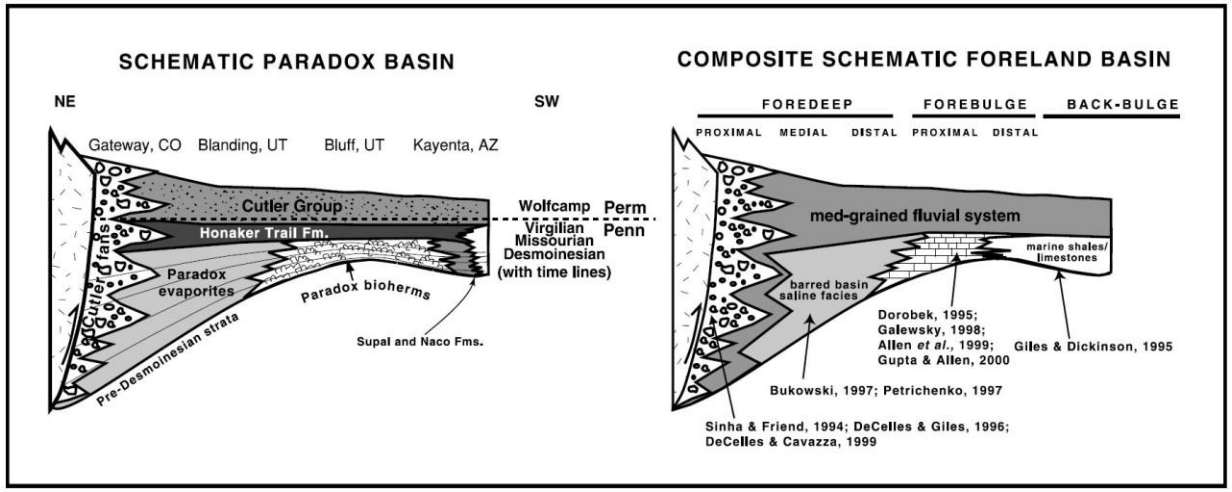

Figure 8. Schematic of the Paradox basin shown as an intraforeland flexural basin relative to the convergence of North America and South America during the Pennsylvanian. The Uncompahgre fault to the NE is the source of sediments that make up the Honaker Trail Formation and Cutler Group. Nearest to the Uncompahgre uplift, coarse alluvial fan deposits represent gravity driven sediment deposition that grades into medium grained fluvial deposits of the Cutler Group to the SW (Barbeau, 2003).

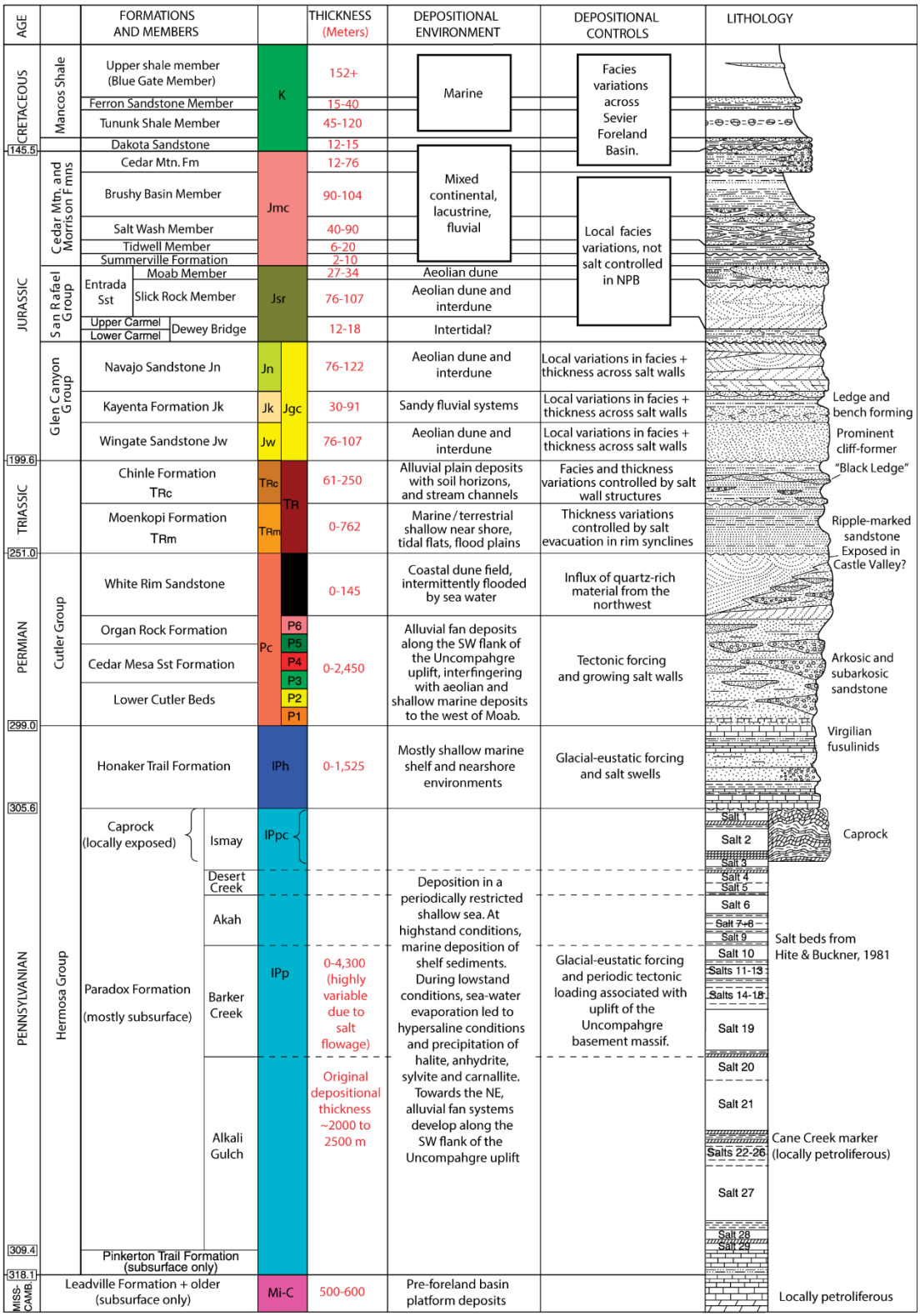

Figure 9. Detailed stratigraphic column of the Onion Creek salt wall taken from Trudgill (2011) and adapted from Doelling and Ross (1998) and Doelling (2002).

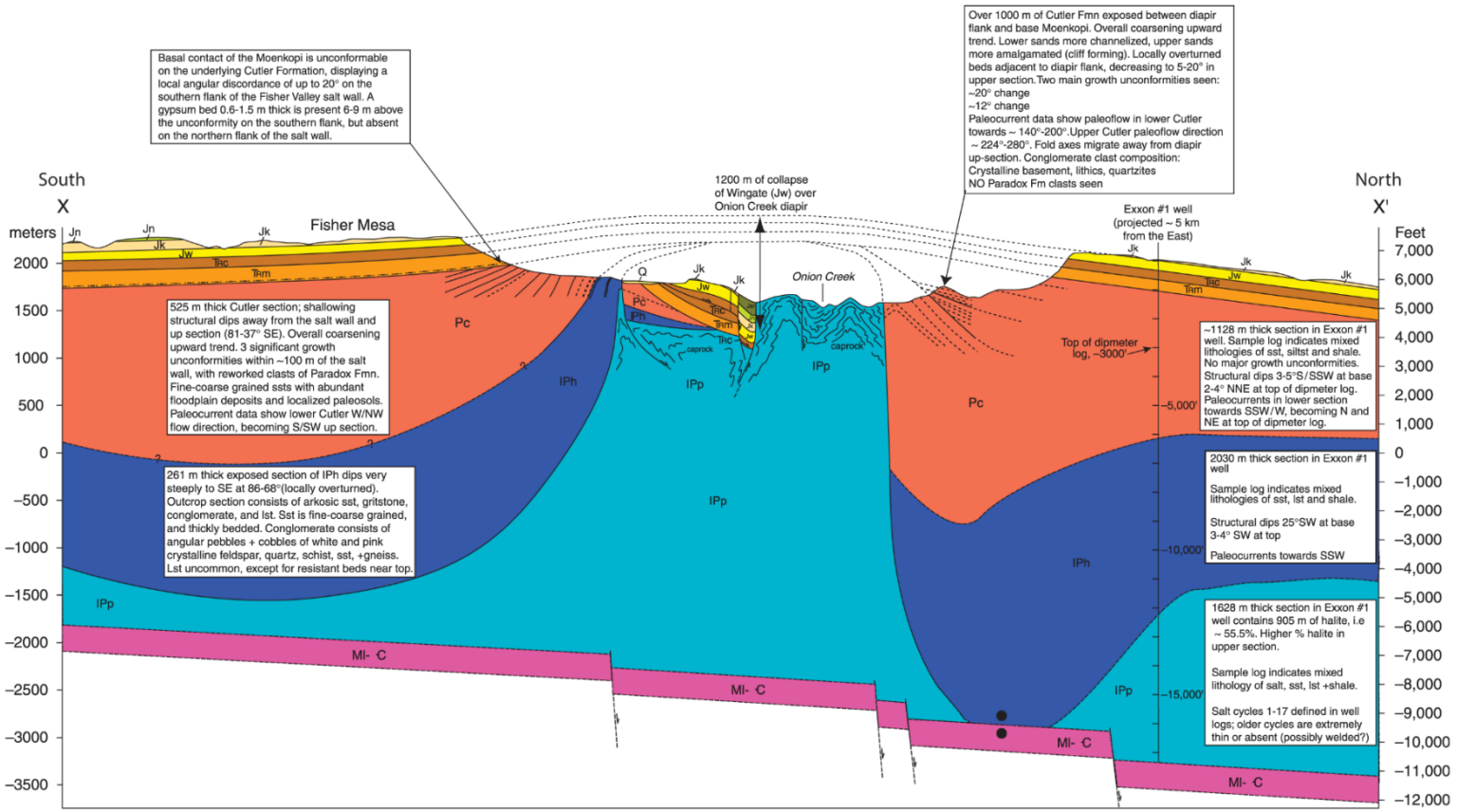

Figure 10. Cross-section from Trudgill (2011) showing the Onion Creek Salt Wall. Thinning of growth strata on the flanks of the Onion Creek salt wall support active salt rise during the Permian. This figure also shows the unconformable contact between the Cutler Group and salts of the Paradox Formation. The Onion Creek Salt Wall is approximately 2.7 km wide.

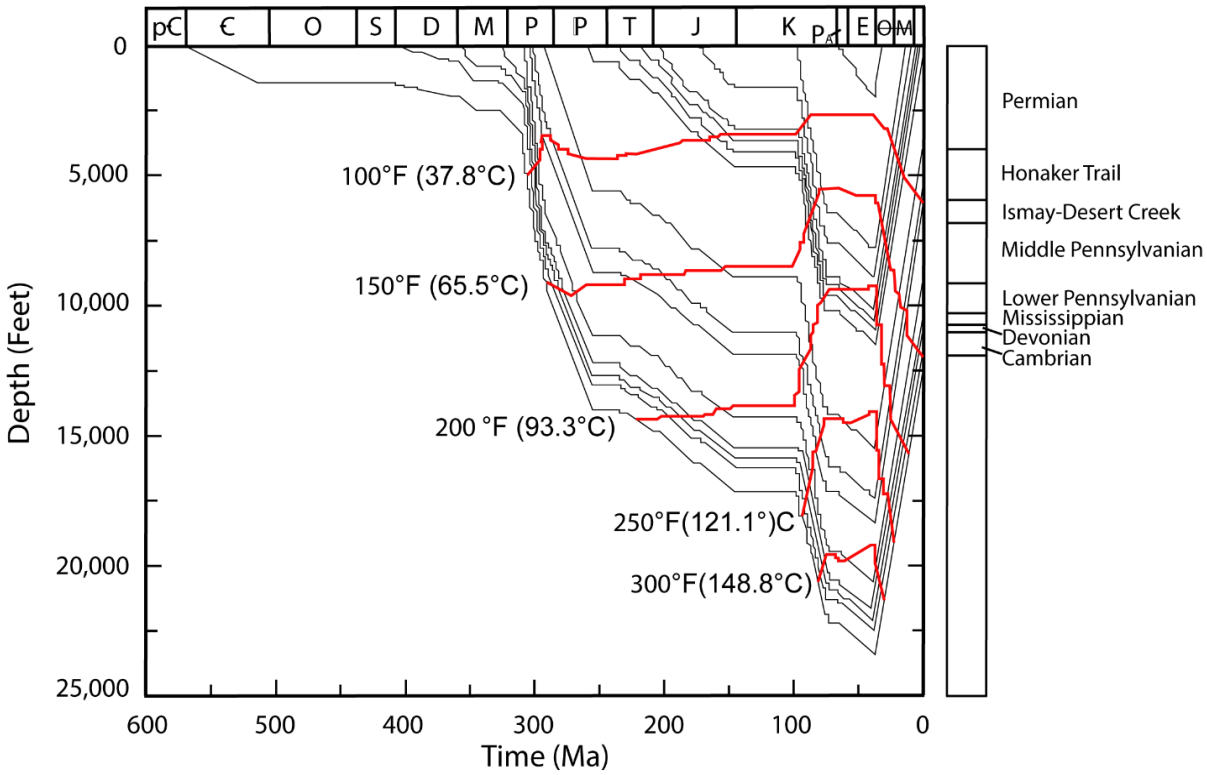

Figure 11. Subsidence curve showing the burial and thermal history of the Paradox Basin near Moab, UT. Temperatures at the top of the Permian Cutler Group are modeled to exceed 93.3˚C (Nuccio and Condon, 1996).

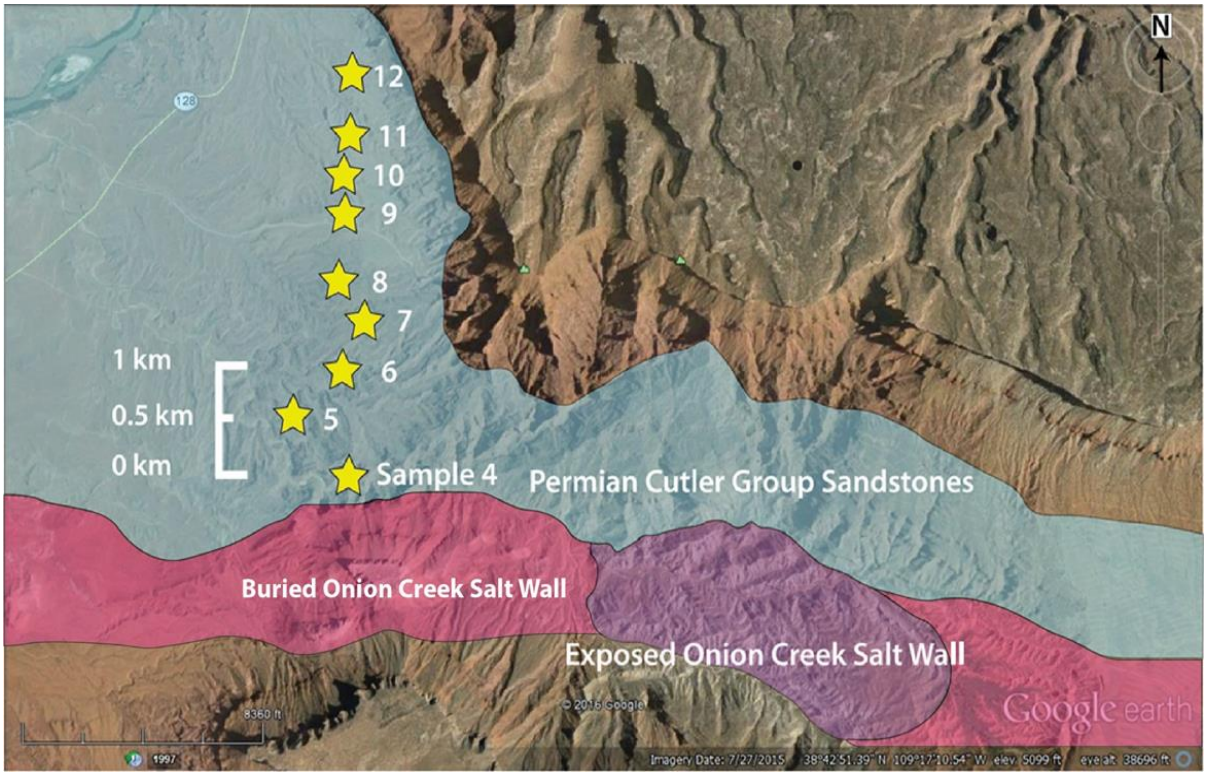

Figure 12. Satellite map showing the location of sample sites in Cutler Group sandstones at Onion Creek, UT. Sample 4 is located at the approximate contact between the Onion Creek salt wall and the Cutler Group. Samples 4 – 12 represent a northerly perpendicular transect with respect to the east-west trending salt wall. Satellite image taken from Google Earth.

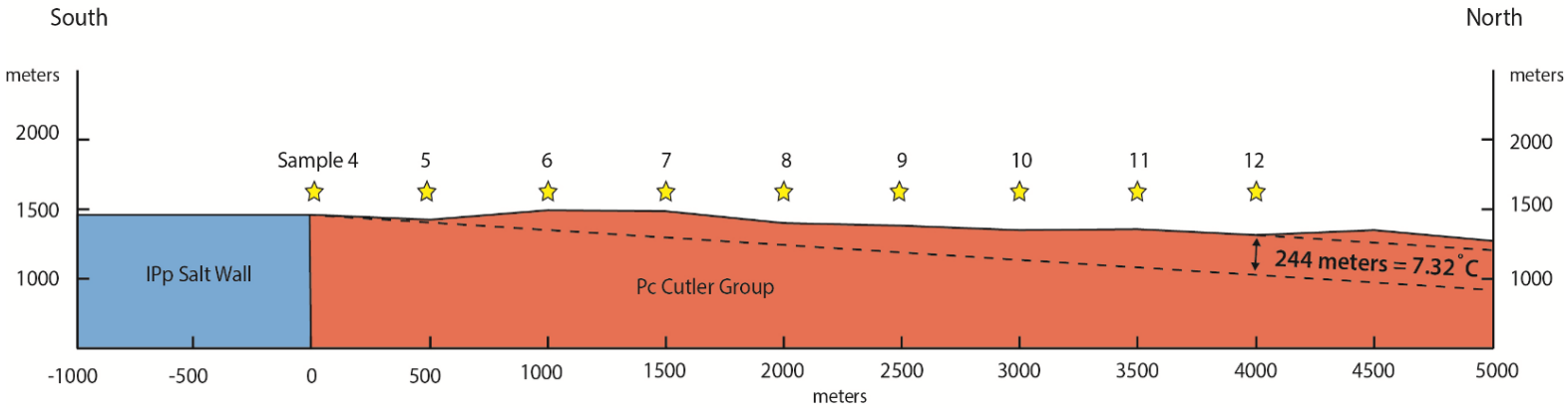

Figure 13. Schematic showing the northerly trending perpendicular transect beginning at sample four near the Onion Creek salt wall (blue) and continuing through the Cutler Group (red). The Cutler Group dips to the north along the perpendicular transect at roughly ~ 3.5˚. We calculated that we climbed 244 meters upward through the Cutler Group stratigraphy beginning at sample four and ending at sample twelve. Elevations were recorded at each sample location site and this schematic does not depict actual elevation changes between sample locations.

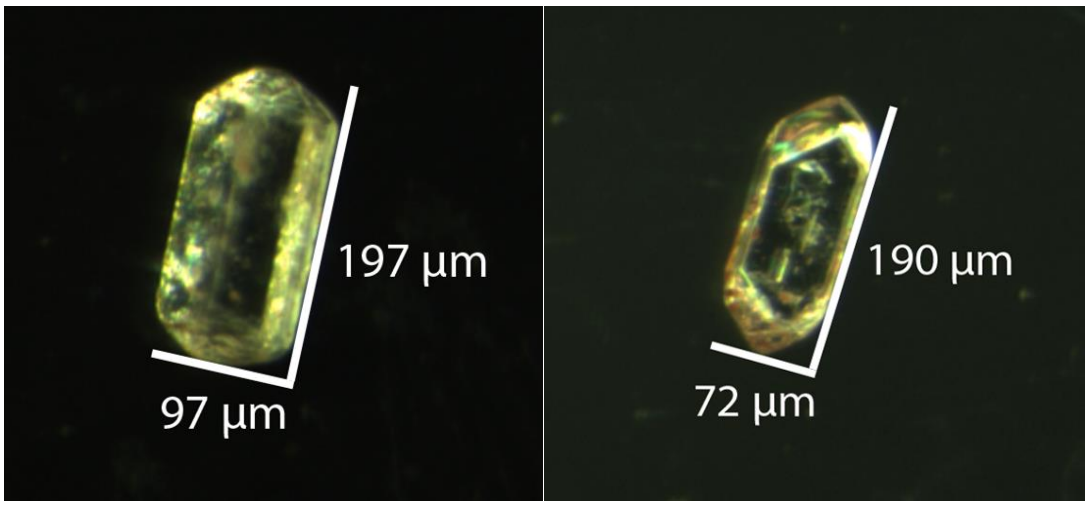

Figures 14 a & b. **(a)** Photomicrograph of an apatite grain with a measured width and height. **(b)** Photomicrograph of a zircon grain with a measured width and height (right).

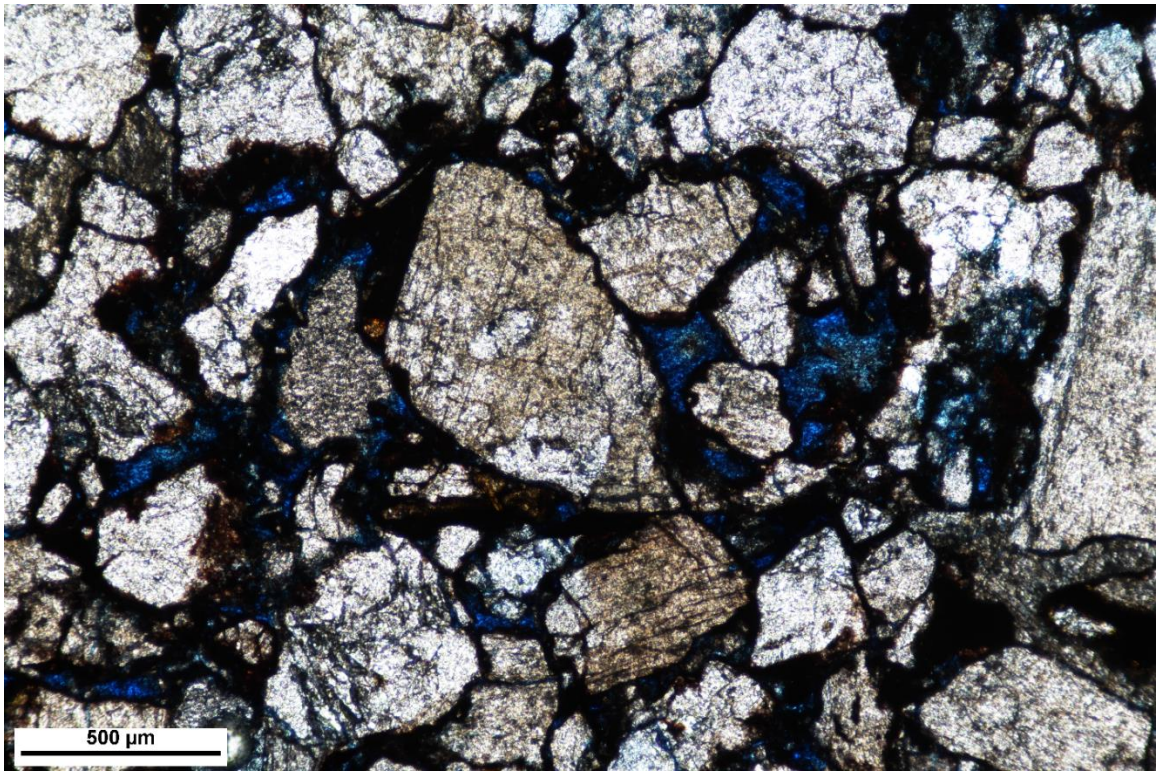

Figure 15. Thin section 15RN08 displaying a large angular Quartz grain roughly 500 µm in diameter in the center of the picture. Pores spaces to the right and left of the quartz grain are also shown in blue.

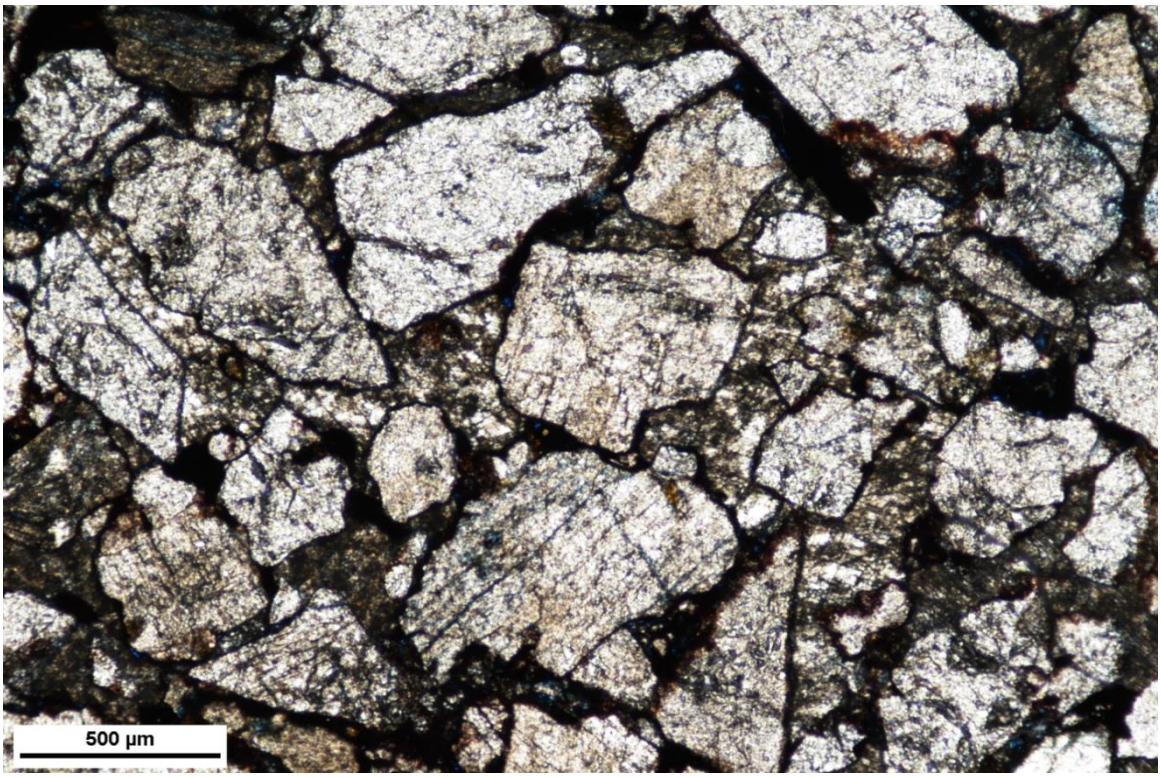

Figure 16. Sample 15RN08 displaying calcite cements between large angular quartz grains. Calcite cement is the most abundant cement observed in these sandstones.

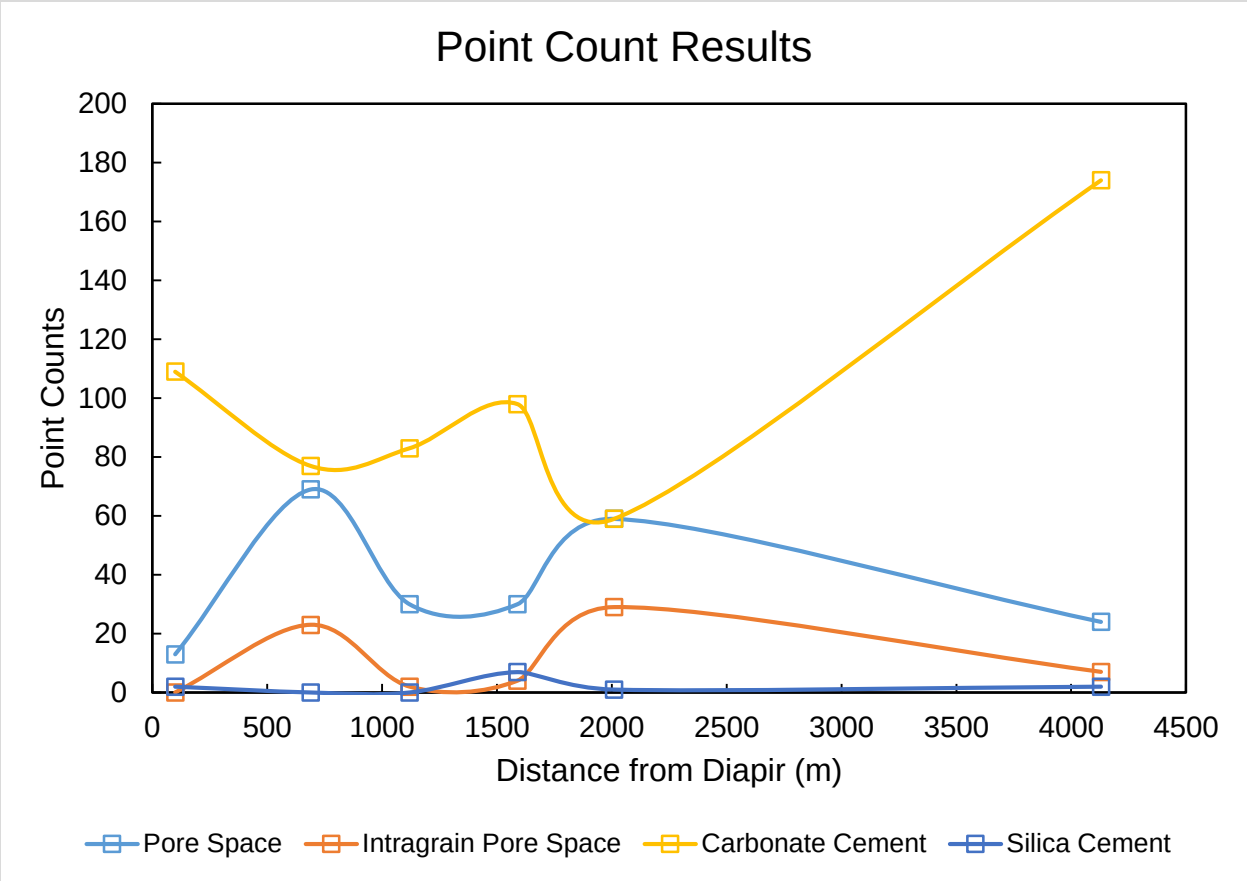

Figure 17. No correlation between pore space, intragrain pore space, carbonate cement, or silica cement and distance from the salt wall is detected.

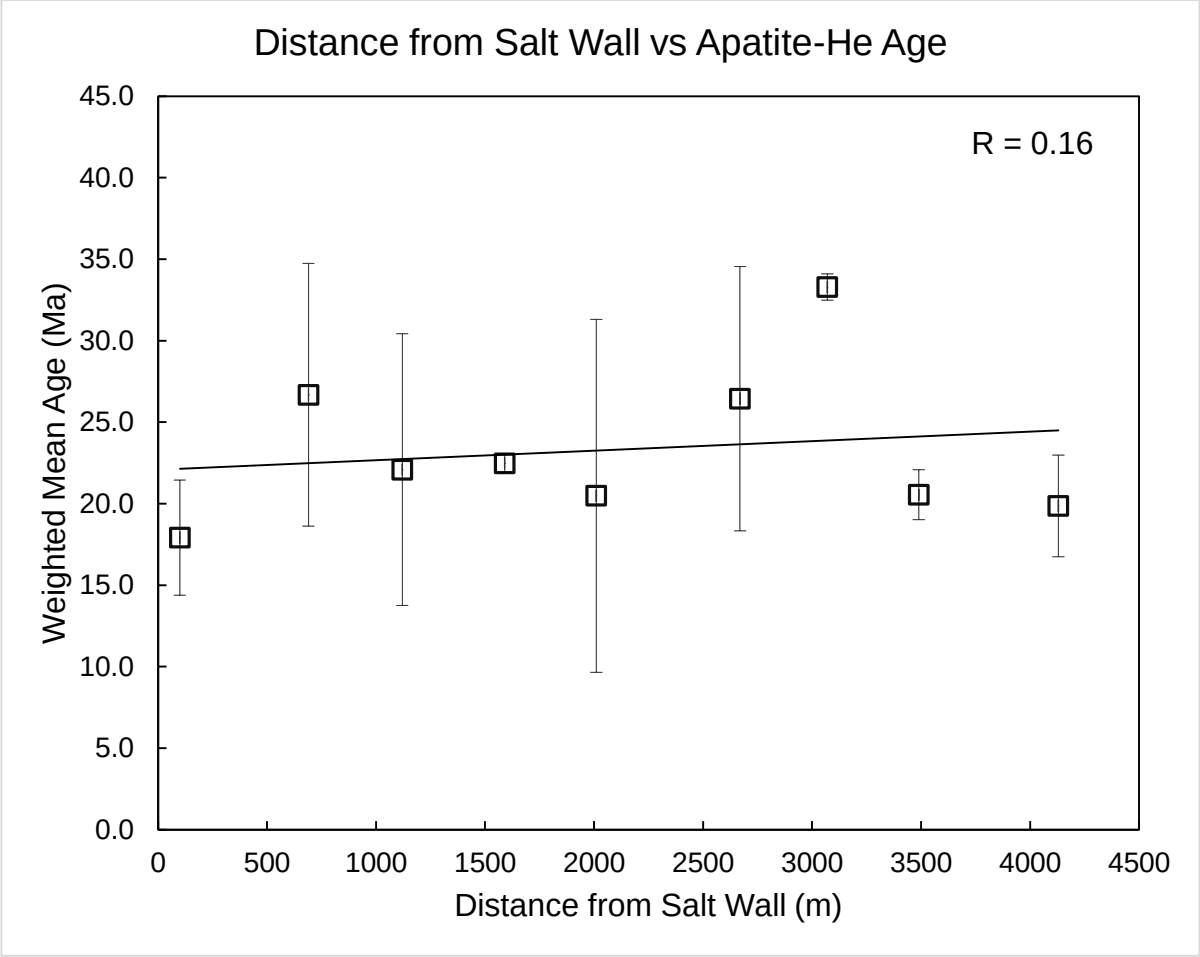

Figure 18. Schematic of apatite-He ages versus distance from the Onion Creek salt wall. No correlation was found between sample apatite-He ages and distance from the Onion Creek salt wall.

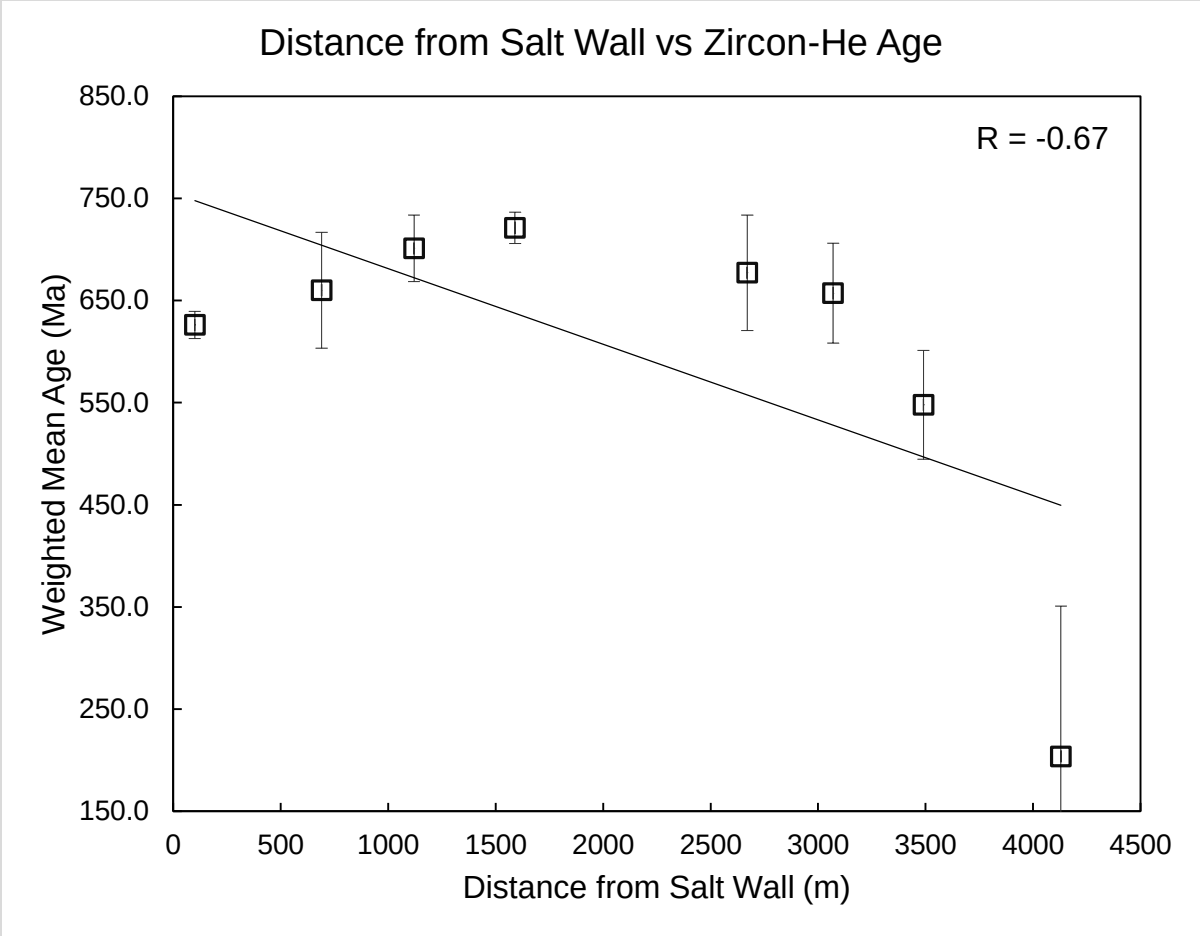

Figure 19. Schematic of Zircon-He ages versus distance from the Onion Creek salt wall.

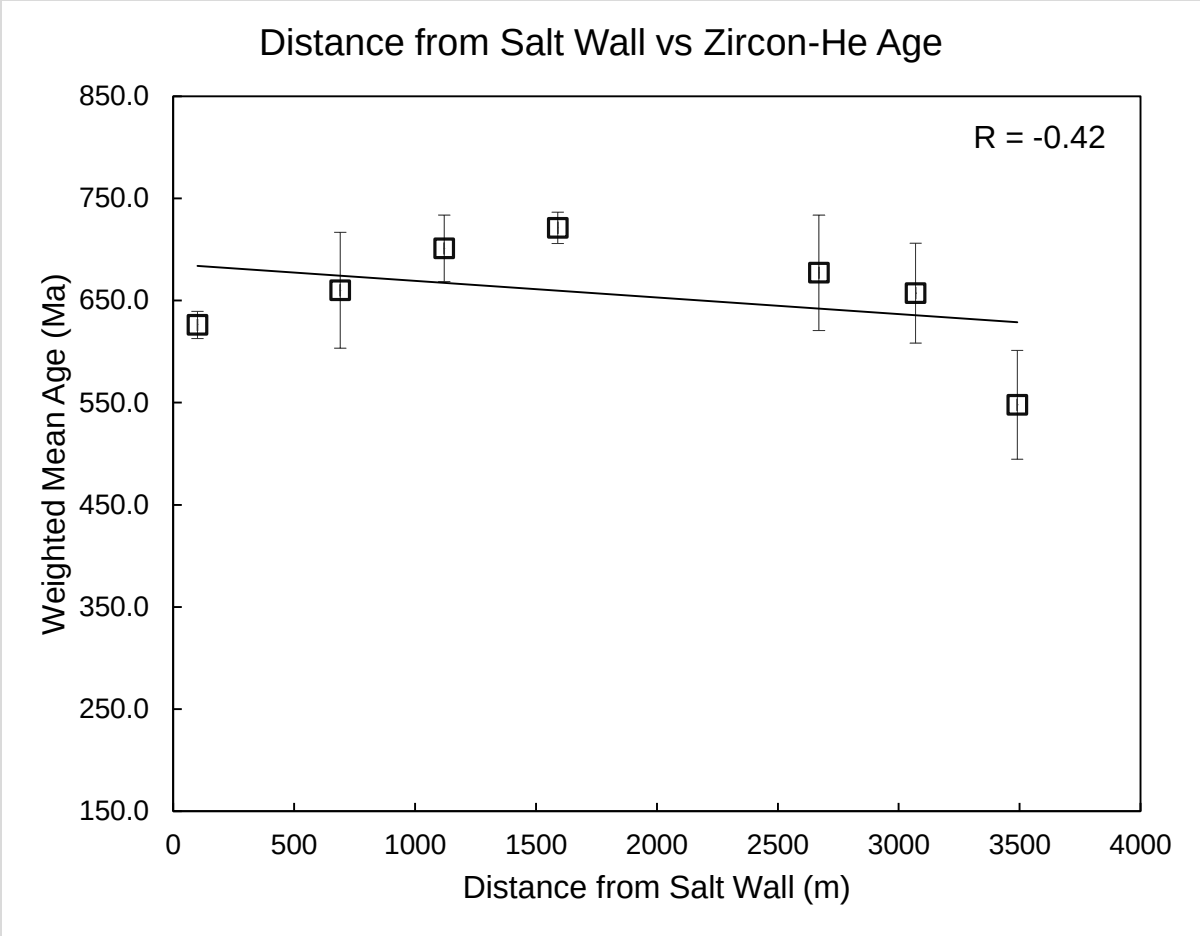

Figure 20. Schematic of zircon-He ages versus distance from the Onion Creek wall excluding sample 15RN12. Sample 15RN12 produced highly dispersed ages and was omitted from this plot.

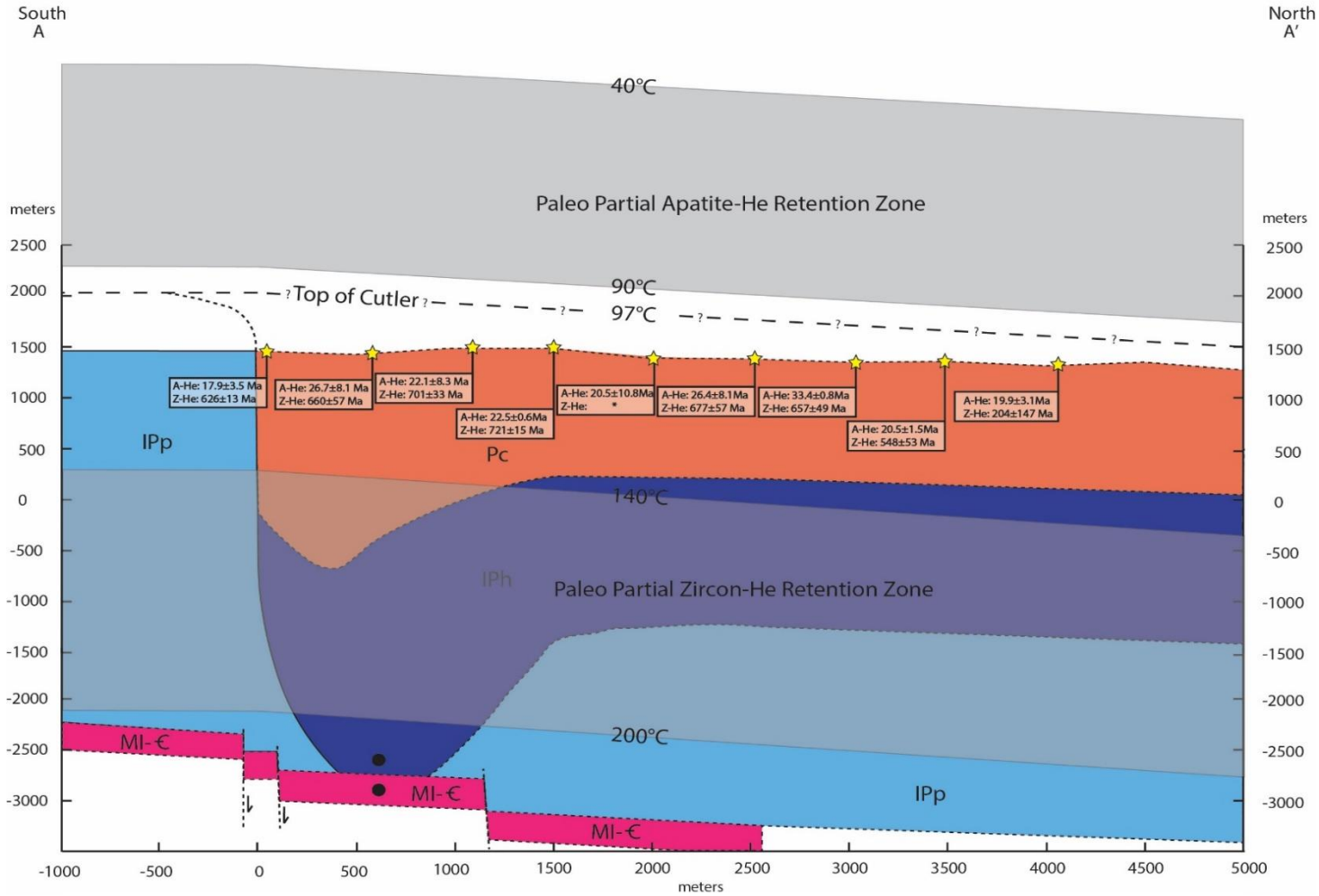

Figure 21. Interpreted Partial He-Retention Temperature Zones, Apatite/Zircon-He Ages, and Sample Location Sites at Onion Creek. Cross-section of the Cutler Group (orange) adjacent to the Onion Creek salt wall (blue) with sample locations and apatite/zircon-He weighted mean ages and associated weighted mean errors shown along the perpendicular sampling transect. Cross-section adapted from Trudgill (2011).

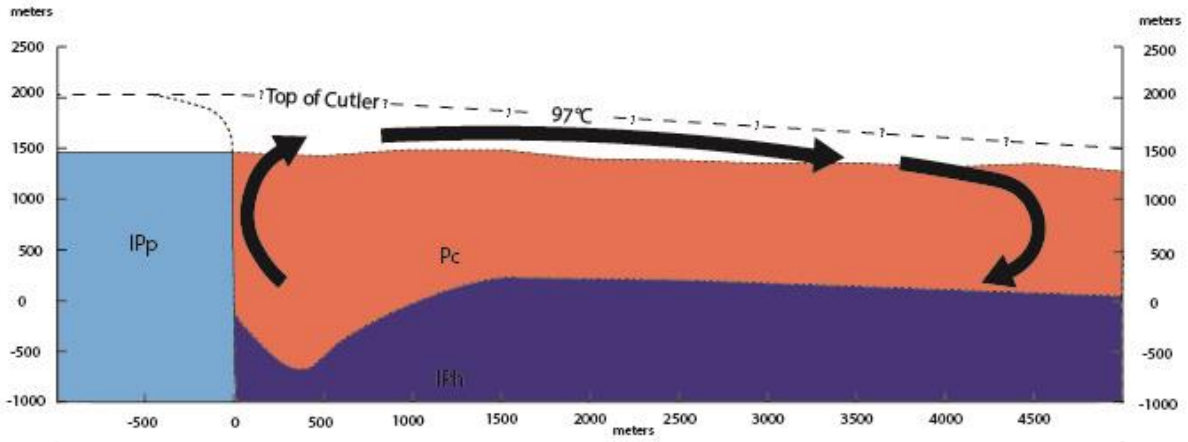

Figure 22. Proposed schematic of the pore fluid flow model that may have homogenized temperatures within the Cutler Group near the Onion Creek salt wall. Arrows indicate direction of fluid flow within the Cutler Group.

LIST OF TABLES

Table 1. Silica cementation analysis results. Samples 15RN09, 15RN10, 15RN11 were omitted from point counts because the samples' grain sizes constituted them as mudstones.

Sample Number	Latitude[a] (°N)	Longtiude[a] (°W)	Elevation (m)	Distance from Diapir (m)	Framework Grains (counts)	Porespace (counts)	Intragrain Porespace (counts)	Matrix (counts)	Carbonate Cement (counts)	Silica Cement (counts)	Dolomite Cement (counts)	Unknown (counts)
15RN04	38.70653	109.31527	1415	100	338	13	0	33	109	2	1	4
15RN05	38.71159	109.32224	1395	690	264	69	23	65	77	0	0	2
15RN06	38.71558	109.31625	1433	1120	292	30	2	91	83	0	0	0
15RN07	38.71971	109.31408	1429	1590	296	30	4	65	98	7	0	0
15RN08	38.72327	109.31728	1381	2010	321	59	29	31	59	1	0	0
15RN12	38.74201	109.31690	1333	4130	245	24	7	48	174	2	0	0

[a]WGS 1984 Datum

Table 2. Apatite-He weighted mean age results.

Sample Name	Latitude[a] (°N)	Longitude[a] (°W)	Elevation (m)	Distance from Diapir (m)	Age[b] (Ma)	MSWD[c]	±2σ[d]	Aliquots[f]
15RN04	38.70653	109.31527	1415	100	17.9	133	3.5[e]	3
15RN05	38.71159	109.32224	1395	690	26.7	339	8.1[e]	3
15RN06	38.71558	109.31625	1433	1120	22.1	298	8.3[e]	3
15RN07	38.71971	109.31408	1429	1590	22.5	0.37	0.6	2
15RN08	38.72327	109.31728	1381	2010	20.0	603	11.0[e]	3
15RN09	38.72919	109.31689	1371	2670	26.4	283	8.1[e]	3
15RN10	38.73265	109.31725	1353	3070	33.3	0.72	0.8	2
15RN11	38.73632	109.31667	1357	3490	20.5	6.59	1.5[e]	2
15RN12	38.74201	109.31690	1333	4130	19.9	70.8	3.1[e]	3

[a]WGS 1984 Datum
[b]Weighted Mean Age excluding outliers determined by the Hampel Identifier
[c]Mean Squared Weighted Devation
[d]Two standard deviation analytical error
[e]Signifies if error expansion was required
[f]Number of dated apatites used in Weighted Mean Age calculation after visual and Hampel Identifier outlier exclusion

Table 3. Zircon-He weighted mean age results.

Sample Name	Latitude[a] (°N)	Longitude[a] (°W)	Elevation (m)	Distance from Diapir (m)	Age[b] (Ma)	MSWD[c]	±2σ[d]	Aliquots[f]
15RN04	38.70653	109.31527	1415	100	626	0.01	13	2
15RN05	38.71159	109.32224	1395	690	660	25	57[e]	3
15RN06	38.71558	109.31625	1433	1120	701	7.05	33[e]	3
15RN07	38.71971	109.31408	1429	1590	721	0.09	15	2
15RN08	38.72327	109.31728	1381	2010	*	*	*	3
15RN09	38.72919	109.31689	1371	2670	677	15.97	57[e]	2
15RN10	38.73265	109.31725	1353	3070	657	18.15	49[e]	3
15RN11	38.73632	109.31667	1357	3490	548	20.83	53[e]	2
15RN12	38.74201	109.31690	1333	4130	204	1409	147[e]	3

[a]WGS 1984 Datum
[b]Weighted Mean Age excluding outliers determined by the Hampel Identifier
[c]Mean Square Weighted Devation
[d]Two standard deviation analytical error
[e]Signifies if error expansion required
[d]Number of dated zircons used in Weighted Mean Age calculation after visual and Hampel Identifier outlier exclusion

Table 4. Raw Apatite-He ages

Sample Name	Aliquot	Radius μm	Length μm	Volume μm³	F_t[a]	^{238}U μmole/g	1σ μmole/g	^{232}Th μmole/g	1σ μmole/g	^{4}He μmole/g	1σ μmole/g	Age[b] Ma	2σ[d]
15RN04	048-4a001	30.7	171.6	420190.2	46.000	0.416526	0.003368	0.438180	0.003842	0.000133	0.000002	15.4	0.45
	048-4a002	36.4	177.6	611360.8	0.650	0.198739	0.001615	0.064716	0.001376	0.005227	0.000070	19.0	0.59
	048-4a003	40.7	211.6	910660.2	0.671	0.090823	0.000781	0.317195	0.002512	0.004533	0.000059	21.4	0.61
15RN05	048-5a001	46.6	201.2	1185922.8	0.702	0.054054	0.000442	0.209983	0.001641	0.002917	0.000038	21.9	0.62
	048-5a002	46.5	192.7	1082528.9	0.700	0.058203	0.000471	0.178394	0.001476	0.004853	0.000060	37.3	1.0
	048-5a003	38.8	177.5	695481.6	0.662	0.822656	0.006699	0.696250	0.005771	0.035266	0.000420	27.9	0.77
15RN06	048-6a001	38.7	231.1	898752.3	0.663	0.089381	0.000753	0.247921	0.002351	0.005238	0.000069	27.7	0.81
	048-6a002	41.4	220.4	981606.1	0.675	0.106168	0.000892	0.420428	0.003399	0.013476	0.000173	51.25	1.45
	048-6a003	48.4	218.5	1331490.6	0.718	0.052215	0.000482	0.102780	0.001285	0.001860	0.000026	18.98	0.60
15RN07	048-7a001	48.4	188.7	1149742.4	0.708	0.068342	0.000613	0.207855	0.001986	0.003394	0.000048	22.6	0.71
	048-7a002	45.2	197.5	1049523.9	0.704	0.475235	0.003734	0.401978	0.003202	0.019004	0.000228	26.0	0.72
	048-7a003	43.8	197.2	984379.8	0.687	0.040080	0.000380	0.125667	0.001723	0.002000	0.000037	22.3	0.89
15RN08	048-8a001	31.0	156.8	391231.6	0.596	0.381270	0.003440	0.220417	0.003787	0.020668	0.000256	37.2	1.1
	048-8a002	38.5	145.6	561203.9	0.646	0.026211	0.000433	0.039597	0.002307	0.001255	0.000034	27.2	1.8
	048-8a003	35.0	136.1	434041.2	0.624	0.458365	0.003669	0.205220	0.003517	0.010791	0.000141	16.6	0.50
15RN09	048-9a001	38.7	180.9	702735.3	0.665	0.265799	0.002105	0.131299	0.002795	0.008413	0.000106	22.1	0.6
	048-9a002	35.6	163.5	538646.2	0.629	0.093900	0.000788	0.183177	0.003647	0.006658	0.000086	37.6	1.2
	048-9a003	32.6	149.9	210.2	0.598	228.014759	2.350835	494.378379	9.312666	12.479743	0.167616	28.2	0.92
15RN10	048-10a001	37.5	181.4	664400.3	0.644	0.107708	0.000871	0.323520	0.003772	0.007827	0.000101	33.1	1.0
	048-10a002	36.3	184.4	631277.8	0.642	0.035692	0.000385	0.056039	0.002853	0.002195	0.000033	33.8	1.4
	048-10a003	33.3	137.8	397717.0	0.603	0.121599	0.001366	0.187258	0.004668	0.003300	0.000051	15.4	0.57
15RN11	048-11a001	43.0	152.8	734593.4	0.664	0.000376	0.000165	0.001938	0.002403	0.011433	0.000138	*[c]	*[c]
	048-11a002	38.1	162.1	610744.1	0.655	0.051545	0.000530	0.027374	0.002908	0.001627	0.000027	21.5	0.9
	048-11a003	41.7	163.7	738420.1	0.680	0.055745	0.000549	0.011870	0.002395	0.001518	0.000021	19.9	0.8
15RN12	048-12a001	41.2	170.3	749093.4	0.676	0.118874	0.000990	0.078978	0.002484	0.003181	0.000042	17.9	0.6
	048-12a002	36.6	159.0	552088.3	0.641	0.088265	0.000859	0.081417	0.003323	0.003326	0.000048	23.9	0.9
	048-12a003	35.2	175.5	564254.1	0.636	0.265290	0.002127	0.203941	0.003559	0.008160	0.000106	20.2	0.60

[a]Mean F_T of $^{238}U_{Ft}$ and $^{232}Th_{Ft}$

[b]Raw (U-Th)/He including F_T correction

[c]* Indicates no calculated (U-Th)/He age and error because isotopic measurements yielded little to no U and Th

[d]Two standard deviation analyitcal error

Table 5. Raw Zircon-He Ages

Sample Name	Aliquot	$Radius_1$ μm	$Radius_2$ μm	$Length_1$ μm	$Height_1$ μm	$Height_2$ μm	Volume μm³	F_T[a] μmole/g	^{238}U μmole/g	1σ μmole/g	^{232}Th μmole/g	1σ μmole/g	^{4}He μmole/g	1σ	Age[b] Ma	2σ[d]
15RN04	048-4z001	29.0	38.4	160.5	25.1	27.3	559146.3	0.707	0.4259	0.0039	0.2512	0.0018	0.4669	0.0055	719.6	10.8
	048-4z002	30.9	30.4	142.3	22.3	24.8	417103.8	0.685	0.7513	0.0064	0.3263	0.0023	0.6891	0.0082	625.6	9.2
	048-4z003	29.0	28.3	142.2	19.4	25.2	369405.8	0.668	0.6109	0.0058	0.3235	0.0017	0.5717	0.0068	626.7	9.5
15RN05	048-5z001	44.0	47.6	265.2	34.6	36.4	1825434.4	0.791	0.6989	0.0061	0.3208	0.0020	0.6473	0.0077	624.8	9.3
	048-5z002	39.1	31.8	228.3	35.6	38.1	892841.4	0.735	0.9142	0.0083	0.3918	0.0022	0.8685	0.0103	646.0	9.8
	048-5z003	37.1	25.9	169.4	23.5	22.4	533795.3	0.693	0.9229	0.0077	0.5683	0.0031	1.0184	0.0121	721.1	10.5
15RN06	048-6z001	31.1	21.4	174.6	23.8	30.5	369193.8	0.646	0.9789	0.0097	0.4257	0.0023	0.9661	0.0115	672.8	10.4
	048-6z002	31.1	29.0	172.7	30.1	22.5	496989.8	0.690	0.6816	0.0057	0.2307	0.0016	0.7193	0.0085	729.1	10.8
	048-6z003	30.6	27.3	164.7	23.5	24.2	443497.8	0.679	0.7469	0.0068	0.3027	0.0018	0.7691	0.0091	703.4	10.7
15RN07	048-7z001	36.3	32.8	228.3	21.3	23.0	946818.2	0.733	0.4833	0.0040	0.2310	0.0012	0.4150	0.0050	580.8	8.6
	048-7z002	31.9	29.7	197.6	21.5	23.2	636689.1	0.702	0.7976	0.0066	0.3902	0.0023	0.8615	0.0103	723.3	10.7
	048-7z003	24.1	29.2	192.0	19.0	18.7	469330.8	0.662	0.6891	0.0067	0.3768	0.0025	0.7461	0.0089	718.8	11.1
15RN08	048-8z001	35.4	27.3	214.4	23.6	28.8	693083.0	0.705	0.7182	0.0060	0.2841	0.0016	1.1363	0.0135	1055.5	16.0
	048-8z002	29.4	29.7	170.2	24.0	19.3	493502.7	0.685	0.5385	0.0046	0.3240	0.0029	0.5412	0.0065	661.3	9.8
	048-8z003	36.8	37.1	213.0	31.8	32.2	930295.7	0.746	2.2607	0.0184	0.4346	0.0030	0.1040	0.0013	34.3	0.5
15RN09	048-9z001	35.5	25.0	205.7	21.3	24.0	623809.0	0.693	0.9262	0.0076	0.3534	0.0020	0.8769	0.0105	651.4	9.6
	048-9z002	32.5	27.7	146.6	27.7	31.2	386396.5	0.643	*c	*c	*c	*c	*c	*c	*c	*c
	048-9z003	31.1	35.0	247.7	24.7	25.9	930972.6	0.724	0.5234	0.0047	0.3537	0.0019	0.5747	0.0068	708.3	10.5
15RN10	048-10z001	31.3	22.3	144.0	24.3	21.2	317204.8	0.644	0.6356	0.0060	0.3189	0.0028	0.6414	0.0076	678.5	10.3
	048-10z002	30.6	28.0	154.6	25.2	22.3	420779.1	0.678	0.9038	0.0081	0.4151	0.0030	0.8179	0.0097	614.8	9.2
	048-10z003	32.4	30.0	133.1	22.8	25.0	393862.8	0.684	0.7739	0.0072	0.3220	0.0027	0.7847	0.0093	691.4	10.5
15RN11	048-11z001	27.2	30.7	167.1	24.8	23.4	451304.1	0.678	0.6475	0.0060	0.4193	0.0020	0.8969	0.0106	891.1	13.5
	048-11z002	29.2	24.9	154.7	28.8	23.7	347028.3	0.655	1.1356	0.0106	0.5618	0.0043	0.9687	0.0115	577.4	8.7
	048-11z003	20.2	23.3	108.3	12.4	19.3	164050.0	0.575	1.1119	0.0106	0.5915	0.0044	0.8611	0.0102	523.9	7.9
15RN12	048-12z001	33.2	32.3	163.1	27.8	27.5	541410.8	0.708	1.1188	0.0103	0.3275	0.0021	1.0696	0.0126	668.7	10.2
	048-12z002	31.2	30.2	167.7	30.7	33.2	471680.5	0.693	1.8849	0.0163	0.3960	0.0025	0.7177	0.0085	278.3	4.1
	048-12z003	42.2	31.2	204.6	33.2	33.9	843430.2	0.737	1.3229	0.0113	0.2374	0.0014	0.2801	0.0033	156.9	2.3

[a]Mean F_T of $^{238}U_{FT}$ and $^{232}Th_{FT}$

[b]Raw (U-Th)/He including F_T correction

[c]* Indicates no calculated (U-Th)/He age and error because isotopic measurements yielded little to no U and Th

[d]Two standard deviation analyitcal error

REFERENCES

Barbeau, D.L., 2003, A flexural model for the Paradox Basin: Implications for the tectonics of the Ancestral Rocky Mountains, Basin Research, v. 15, p. 97 – 115.

Bjorlykke, K., Aagaard, P., Dypvik, H., Hastings, D.S., and Harper, A.S., 1986, Diagenesis and reservoir properties of Jurassic sandstones from the Haltenbanken area, offshore mid Norway, *in* Proceedings, Habitat of Hydrocarbons on the Norwegian Continental Shelf, Norwegian Petroleum Society, Stavanger, Norway, October 1 – 3, 1985, p. 275 – 286.

Cather, S.M., Chapin, C.E., and Kelley, S.A., 2012, Diachronous episodes of Cenozoic erosion in southwestern North America and their relationship to surface uplift, paleoclimate, paleodrainage, and paleoaltimetry: Geosphere, v. 8, p. 1177 – 1206.

Chew, D.M., and Donelick, R.A., 2012, Combined apatite fission track and U-Pb dating by LA-ICP-MS and its application in apatite provenance analysis, *in* Proceedings Mineralogical Association of Canada Short Course 42, May 2012, p. 219 – 247.

Condon, S.M., 1997, Geology of the Pennsylvanian and Permian Cutler Group and Permian Kaibab Limestone in the Paradox Basin, Southeastern Utah and Southwestern Colorado: U.S. Geological Survey Bulletin, no. 2000-P, p. 1 – 59.

Crowley, P.D., Reiners, P.W., Reuter, J.M., and Kaye, G.D., 2002, Laramide Eexhumation of the Bighorn Mountains, Wyoming: An apatite (U-Th)/He thermochronology study, Geology, v. 30, p. 27 – 30.

Donelick, R.A., O'Sullivan, P.B., and Ketcham, R.A., 2005, Apatite fission-track analysis: Reviews in Mineralogy and Geochemistry, v. 58, p. 49 – 94.

Doelling, H.H., and Ross, M.L., 1998, Geologic map of the Big Bend quadrangle, Grand County, Utah: Utah Geological Survey Map 171, p. 29, scale 1:24,000.

Doelling, H.H., 2002, Geologic map of the Fisher Towers 7.5' Quadrangle, Grand County, Utah: Utah Geological Survey Map 181, p. 34, scale 1:24,000.

Ehlers, T.A., and Farley, K.A., 2003, Apatite (U-Th)/He thermochronometry: Methods and applications to problems in tectonic and surface processes, Earth and Planetary Science Letters, v. 206, p. 1 – 14.

Evans, D.G., and Nunn, J.A., 1989, Free thermohaline convection in sediments surrounding a salt column: Journal of Geophysical Research, v. 94, p. 413 - 422.

Evans, D.G., Nunn, J.A., and Hanor, J.S., 1991, Mechanisms driving groundwater flow near salt domes: Geophysical Research Letters, v. 18, p. 927 – 930.

Evans, S. L., R. H. Styron, M. C. van Soest, K. V. Hodges, and A. D. Hanson, 2015, Zircon and apatite (U-Th)/He evidence for Paleogene and Neogene extension in the Southern Snake Range, Nevada, USA: Tectonics, v. 34, p. 2142–2164, doi:10.1002/2015TC003913.

Evans, S.L., 2015, Personal Communication.

Evans, S.L., 2016, (U-Th)/He Studies of the Southern Snake Range Metamorphic Core Complex, NV and Gypsum Valley Salt Wall, Paradox Basin, CO, USA [Ph.D. dissertation]: Las Vegas, University of Nevada.

Farley, K.A., Wolf, R.A., and Silver, L.T., 1996, The effects of long alpha-stopping distances on (U-Th)/He ages: Geochimica et Cosmochimica Acta, v. 60, p. 4223 – 4229.

Flowers, R.M., Wernicke, B.P., and Farley, K.A., 2003, Unroofing, incision, and uplift History of the southwestern Colorado Plateau from apatite (U-Th)/He thermochronometry: Geological Society of America Bulletin May/June 2008, v. 120, p. 571 – 587.

Griffin, D.E., 1989, Theoretical and numerical models for heat and mass transport and groundwater flow near salt domes [Ph.D dissertation]: Louisiana State University.

Geertsma, J., 1971, Finite-element analysis of shallow temperatures anomalies: Geophysical Prospecting 19, p. 662 – 681.

Hampel, F.R., 1971, A general qualitative definition of robustness: The annals of mathematical statistics, v. 42, p. 1887 – 1896.

Hanor, J.S., and Workman, A.L., 1986, Distribution of dissolved volatile fatty acids in some Louisiana oil field brines: Applied Geochemistry, v. 1, p. 37 – 46.

Hanor, J.S., 1987, Kilometre-scale thermohaline overturn of pore waters in the Louisiana Gulf Coast: Nature, v. 327, p. 501 – 503.

Hansen, W.R., and Peterman, Z.E., 1968, Basement-rock geochronology of the black canyon of the Gunnison, Colorado: Geological Survey Research Prof. Paper 600-C, p. C80 – C90.

Hanson, A. D., 2014, A surprising asymmetric paleothermal anomaly around El Gordo diapir, La Popa Basin, Mexico: American Association of Petroleum Geologists Bulletin, v. 96, p. 213 – 226.

Hedge, C.E., Peterman, Z.E., Case, J.E., and Obradovich, J.D., 1968, Precambrian geochronology of the northwestern Uncompahgre Plateau, Utah and Colorado: Geological Survey Research Professional Paper 600-C, p. 91 – 96.

Hite, R.J., and Buckner, D.H., 1981, Stratigraphic correlations, facies concepts, and cyclicity in Pennsylvanian rocks of the Paradox Basin: Rocky Mountain Association of Geologists 1981 Field Conference, p. 147 – 159.

Hoffman, M.D., 2009, Mio-Pliocene erosional exhumation of the central Colorado Plateau, Eastern Utah: New insights from apatite (U-Th)/He thermochronometry [Master's thesis], University of Kansas.

Hourigan, J.K., Reiners, P.W., and Brandon, M.T., 2005, U-Th zonation-dependent alpha-ejection in (U-Th)/He chronometry: Geochimica et Cosmochimica Acta, v. 69, p. 3349 – 3365.

Hudec, M. R., 1995, The Onion Creek salt diapir: an exposed diapir fall structure in the Paradox Basin, Utah, *in* Proceedings, GCSSEPM Foundation 16th Annual Research Conference Salt, Sediment and Hydrocarbons, December 3-6, 1995.

Jackson, M., 1998, Processes of laccolithic emplacement in the southern Henry Mountains, Southeastern Utah: U.S. Geological Survey Bulletin 2158, p. 52 – 58.

Jensenius, J., and Munksgaard, N.C., 1988, Large scale hot water migration systems around salt diapirs in the Danish Central Trough and their impact on diagenesis of chalk reservoirs: Geochimica et Cosmochimica Acta, v. 53, p. 79 – 88.

Jensen, P.K., 1983, Calculations of the thermal conditions around a salt diapir: Geophysical Prospecting, v. 31, p. 481 – 489.

Kluth, C.F., and DuChene, H.R., 2009, Late Pennsylvanian and early Permian structural geology and tectonic history of the Paradox Basin and Uncompahgre Uplift, Colorado and Utah:

in Houston et al., The Paradox Basin Revisited – New Developments in Petroleum Systems and Basin Analysis: 2009 RMAG Special Publication, p. 178-197.

Land, L.S., and Fisher, S.R., 1987, Wilcox sandstone diagenesis, Texas Gulf Coast: a regional isotopic comparison within the Frio Formation: Geological Society Special Publication, v. 36, p. 219 – 235.

Langford, R., and Chan, M.A., 1988, Flood surfaces and deflation surfaces within the Cutler Formation and Cedar Mesa Sandstone (Permian), southeastern Utah: Geological Society of America Bulletin, v. 100, p. 1541 – 1549.

Lawton, T.F. and Buck, B.J., 2006, Implications of diapir-derived detritus and gypsic paleosols in Lower Triassic strata near the Castle Valley salt wall, Paradox Basin, Utah: Geological Society of America, v. 34, p. 885 – 888.

Leger, W.T., 1988, Salt dome related diagenesis of Miocene sediment; Black Bayou Field, Cameron Parish, Louisiana: Trans. Gulf Coast Association of Geologists Society, v. 28, p. 525 – 534.

Mack, G.H., 1977, Depositional environments of the Cutler-Cedar Mesa Facies transition (Permian) near Moab, Utah: The Mountain Geologist, v. 14, p. 53 – 68.

Mack, G.H., and Rasmussen, K.A., 1984, Alluvial-fan sedimentation of the Cutler Formation (Permo-Pennsylvanian) near Gateway, Colorado: Geological Society of America Bulletin, v. 95, p. 109 – 116.

McBride, E.F., 1989, Quartz Cement in sandstones: a review, Earth-Science Reviews, v. 26, p. 69 – 112.

McMillan, M.E., Heller, P.L., Wing, S.L., 2006, History and causes of post-Laramide relief in the Rocky Mountain orogenic plateau: Geological Society of America Bulletin March/April 2006, v. 118, p. 392 – 405.

Mello, U.T., Karner, G.D., and Anderson, R.N., 1995, Role of salt in restraining the maturation of subsalt source rocks: Marine and Petroleum Geology, v. 12, p. 697 – 716.

Murray, K.E., Orme, D.A., and Reiners, P.W., 2011, Apatite (U-Th)/He date dispersion due to secondary grain boundary phases: An example from the Henry Mountains, Utah, *in* Proceedings, American Geophysical Union Fall Meeting 2011, abstract#V23A-2556.

Nagihara, S., 2003, Three-dimensional inverse modeling of the refractive heat-flow anomaly associated with salt diapirism: American Association of Petroleum Geologists Bulletin, v. 87, p. 1207 – 1222.

Nuccio, V.F., and Condon, S.M., 1996, Burial and thermal history of the Paradox Basin, Utah and Colorado, and petroleum potential of the Middle Pennsylvanian Paradox Formation: U.S. Geological Survey Bulletin 2000-O, p. 1 – 41.

O'Brien, J.J., and Lerche, I., 1984, The influence of salt domes on paleotemperature distributions: Geophysics, v. 49, p. 2032 – 2043.

Ohlen, H.R., McIntyre, L.B., 1965, Stratigraphy and tectonic features of Paradox Basin, Four Corners Area: American Association of Petroleum Geologists Bulletin, v. 49, p. 2020 – 2040.

Pederson, J.L., Callahan, C.N., and Roy, M., 2007, The central Colorado Plateau bullseye – linking patterns of quantified incision, exhumation, and flexure: Geological Society of America Abstracts with Programs, v. 39, p. 194.

Petersen, K., and Lerche, I., 1995, Quantification of thermal anomalies in sediments around salt structures: Geothermics. v. 24, p. 253 – 268.

Pettijohn, F.J., 1975, Sedimentary Rocks (3rd edition). Harper and Row, New York.

Peyton, S.L., Reiners, P.W., Carrapa, B., and DeCelles, P.G., 2012, Low-temperature thermochronology of the Northern Rocky Mountains, Western U.S.A.: American Journal of Science, v. 312, p. 145 – 212.

Peyton, S.L., and Carrapa, B., 2013, An introduction to low-temperature thermochronologic techniques, methodology, and applications, in C. Knight and J. Cuzella, eds., Application of structural methods to Rocky Mountain hydrocarbon exploration and development: AAPG Studies in Geology, v. 65, p. 15–36.

Ranganathan, V., 1992, Basin dewatering near salt domes and formation of brine plumes: Journal of Geophysical Research, v. 97, p. 4667 – 4683.

Rahl, J.M., Reiners, P.W., Campbell, I.H., Nicolescu, S., and Allen, C.M., 2003, Combined single-grain (U-Th)/He and U/Pb dating of detrital zircons from the Navajo Sandstone, Utah: Geology, v. 31, p. 761 – 764.

Rashid, M.A. and McAlar, J.D., 1977, Early maturation of organic matter and genesis of hydrocarbons as a result of heat from a shallow piercement salt dome: Journal of Geochemical Exploration, v. 8, p. 549 – 569.

Reiners, P.W., 2005, Zircon (U-Th)/He thermochronometry: Reviews in Mineralogy & Geochemistry, v. 58, p. 151 – 179.

Reiners, P.W., Campbell, I.H., Nicolescu, S., Allen, C.M., Hourigan, J.K., Garver, J.I., Mattinson, J.M., and Cowan, D.S., 2005, (U-Th)/(He-Pb) double dating of detrital zircons: American Journal of Science, v. 305, p. 259 – 311.

Roberts, G.G., White, N.J., Martin-Brandis, G.L., and Crosby, A.G., 2012, An uplift history of the Colorado Plateau and its surroundings from inverse modeling of longitudinal river profiles: Tectonics, v. 91, TC4022.

Ronnevik, C., Ksienzyk, A.K., Fossen, H., Jacobs, J., Dunkl, I., and Bea, F., 2014, Thermochronology of the Uncompahgre Plateau and La Sal Mountains: new apatite fission track, (U-Th)/He and zircon U/Pb data, *in* Proceedings, 14th International Conference on Thermochronology, Chamonix-Mont Blanc, France.

Rowan, M.G., Lawton, T.F., Giles, K.A., and Ratliff, R.A., 2003, Near-salt deformation in La Popa basin, Mexico, and the northern Gulf of Mexico: A general model for passive diapirism: America Association of Petroleum Geologists Bulletin, v. 87, p. 733 – 756.

Schmoker, J.W., and Gautier, D.L., 1988, Sandstone porosity as a function of thermal maturity: Geology, v. 16, p. 1007 – 1010.

Selig, F., and Wallick, G.C., 1966, Temperature distribution in salt domes and surrounding sediments: Geophysics, v. 31, p. 346 – 361.

Shuster, D.L., Flowers, R.M., Farley, and K.A., 2006, The influence of natural radiation damage on helium diffusion kinetics in apatite: Earth and Planetary Science Letters, v. 249, p. 148 – 161.

van Soest, M.C., Hodges, K.V., Wartho, J., Biren, M.B., Monteleone, B.D., Ramezani, J., Spray, J.G., and Thompson, L.M., 2011, (U-Th)/He dating of terrestrial impact structures: The Manicouagan example, Geochemistry, Geophysics, and Geosystems, v. 12, p. 1 – 8.

Stern, T.W., Newell, M.F., Kistler, R.W., and Shawe, D.R., 1965, Zircon uranium-lead and thorium-lead ages and mineral potassium-argon ages of La Sal Mountains rocks, Utah: Journal of Geophysical Research, v. 70, p. 1503 – 1507.

Stock, G.M., Ehlers, T.A., and Farley, K.A., 2006, Where does sediment come from? Quantifying catchment erosion with detrital apatite (U-Th)/He thermochronometry: Geology, v. 34, p. 725 – 728.

Stockli, D.F., Farley, K.A., and Dumitru, T.A., 2000, Calibration of the apatite (U-Th)/He thermochronometer on an exhumed fault block, White Mountains, California: Geology, v. 28, p. 983 – 986.

Stockli, D.F., Surpless, B.E., and Dumitru, T.A., 2002, Thermochronological constraints on the timing and magnitude of Miocene and Pliocene extension in the Central Wassuk Range, Western Nevada: Tectonics, v. 21, p. 1 – 19.

Sullivan, K.R., Kowallis, B.J., and Mehnert, H.H., 1991, Isotopic ages of igneous intrusions in Southeastern Utah: Evidence for a Mid-Cenozoic Reno – San Juan Magmatic Zone: BYU Geology Studies 1991, v. 37, p. 139 – 144.

Trudgill, B.D., 2011, Evolution of salt structures in the northern Paradox Basin: controls on evaporate deposition, salt wall growth and supra-salt stratigraphic architecture: Basin Research, v. 23, p. 208 – 238.

Vendeville, B.C., and Jackson, M.P.A., 1992a, The rise of diapirs during thin-skinned extension: Marine and Petroleum Geology, v. 9, p. 331 – 353.

Vizgirda, J., O'Brien, J.J., and Lerche, I., 1985, Thermal anomalies on the flanks of a salt dome: Geothermics, v. 14, p. 553 – 565.

Walderhaug, O., 1994, Temperatures of quartz cementation in Jurassic Sandstones from the Norwegian Continental Shelf – Evidence from fluid inclusions: Journal of Sedimentary Research, v. A64, p. 311 – 323.

Wendt, I., Carl, C., 1991, The statistical distribution of the mean squared weighted deviation: Chemical Geology, v. 86, p. 275 – 285.

Wells, M.L., Dallmeyer, R.D., and Allmendinger, R.W., 1990, Late Cretaceous extension in the hinterland of the Sevier Thrust Belt, Northwestern Utah and Southern Idaho: Geology, v. 18, 929 – 933.

Wolf, R.A., Farley, K.A., and Silver, L.T., 1996, Helium diffusion and low-temperature thermochronometry of apatite: Geochimica et Cosmochimica Acta, v. 60, p. 4231 – 4240.

Wolf, R.A., Farley, K.A., and Kass, D.M., 1998, Modeling of the temperature sensitivity of the apatite (U-Th)/He thermochronometer: Chemical Geology, v. 148, p. 105 – 114.

Wolfe, M.R., and Stockli, D.F., 2010, Zircon (U-Th)/He thermochronometry in the KTB Drill Hole, Germany, and its implications for bulk He diffusion kinetics in zircon: Earth and Planetary Science Letters, v. 295, p. 69 – 82.

Ye, H., Royden, L., Burchfiel, C., and Schuepbach, M., 1996, Late Paleozoic deformation of interior North America: The greater Ancestral Rocky Mountains, American Association of Petroleum Geologists Bulletin, v. 80, p. 1397 – 1432.

Yonkee, W.A., Dehler, C.D., Link, P.K., Balgord, E.A., Keeley, J.A., Hayes, D.S., Wells, M.L., Fanning, C.M., and Johnston, S.M., 2014, Tectono-stratigraphic framework of Neoproterozoic to Cambrian strata, west-central U.S.: Protracted rifting, glaciation, and evolution of the North American Cordilleran margin: Earth-Science Reviews, v. 136, p. 59 – 95.

Yu, Z., Lerche, I., and Lowrie, A., 1992, Thermal impact of salt: Simulation of thermal anomalies in the Gulf of Mexico: PAGEOPH, v. 138, p. 181 – 192.

CURRICULUM VITAE

Richard Gregory Ness

Education

University of Nevada Las Vegas
Master of Science in Geoscience
GPA: 3.96/4.0
Graduation December 2016
Thesis Adviser: Andrew D. Hanson

University of Tennessee Knoxville
Bachelor of Science in Geology
GPA: 3.61/4.0
Cum Laude
Graduated July 2014
Research Adviser: Joshua P. Emery

Professional Experience

- ExxonMobil Development/Production Internship (May 24, 2016 – August 20, 2016)
  - Intern Project - Seismic depth uncertainty assessment on two assets located in the Gulf of Mexico
  - Utilized Petrel (3D geologic spatial software) to map regions of seismic depth uncertainty along a hydrocarbon bearing reservoir
  - Earned experience interpreting geologic models on 3D seismic volumes and used velocity modeling to enhance seismic data accuracy
- ExxonMobil Geoscience Recruiting Field Course, Bighorn Basin, Wyoming (July 13 – 20, 2014)
  - Conduct Integrated basin & hydrocarbon play element analysis in Bighorn Basin
  - Create a unique play concept in the Bighorn Basin with a team of geoscientists
  - Present play concept to management with cross-sections and hydrocarbon systems maps

---

Master's Thesis

- Salt Thermal Anomalies Research (January 2015 – Present)
  - Testing for paleothermal anomaly in a sandstone reservoir adjacent to a salt wall, Paradox Basin, Utah – has implications for reducing exploration risk in salt basins (Corporate Sponsors – Chevron/ConocoPhillips)
  - Conducted field sampling and laboratory work using (U-Th)/He Thermochronometry
  - Conclusions – Key learnings are proprietary (Corporate Sponsor Agreement) but results have implications for constraining sedimentary uplift associated with La Sal Igneous Intrusion and Neoproterozoic Exhumation in Southern Utah

Research (Undergraduate)

- ❖ Near-Infrared Spectroscopy of the Trojan Asteroids (May 2012–May 2013)
  - Used data from the NASA Infrared Telescope Facility to test the distribution of spectral types within Jupiter's Trojan Asteroid population
  - Presented a poster at the Division of Planetary Sciences Conference of 2012 in Reno, NV
- ❖ Thermal Inertia Estimates of Near-Earth Asteroids (May 2013–December 2014)
  - Used thermal infrared data from the NASA Spitzer Space Telescope to estimate thermal inertias of four near-earth asteroids
  - Presented poster at the Lunar Planetary Science Conference of 2014 in Houston

---

Field Experience

- ❖ University of South Dakota School of Mines and Technology Summer 2014 Field Camp, Turkey (June 1 – July 5)
  - Conduct field mapping along the North Anatolian Fault Zone (NAFZ)
  - Reconstructed the stratigraphic framework of the Abant & Yenipazar Formations
  - Map complex geologic structures and define the geologic history of a segment of the North Anatolian Fault
- ❖ Salt Tectonics Short Course (May 2015)
  - Salt/sediment workshop aimed at learning about evolution/uncertainties in reservoirs adjacent to subsurface salt structures (Univ. of Texas El Paso)

Software Experience

- Petrel – Three months experience interpreting 3-D Seismic Volumes (ExxonMobil Internship)
- ArcGIS (Geographic Information Systems) – Eight months experience (Univ. of Nevada, Las Vegas & ExxonMobil Internship)
- RockDoc – One month experience cross-plotting well data (ExxonMobil Internship)
- RockWare – Three months experience creating stratigraphic columns and location maps (Univ. of Nevada, Las Vegas)
- IDL (Information Data Language) – Three years experience coding (Univ. of Tennessee)
- Matlab – Six months experience coding during a calculus course (Univ. of Tennessee)

Awards

- Natural Sciences Teaching Assistantship Scholarship *2015*
- Outstanding Senior Award in Geology *2014*
- Courage to Climb Aware for Research, Leadership, Service and Civility *2013*
- Professional Promise Award *2013*
- McClung Museum Teach Outreach Service Award *2013*
- Otto Kopp Scholarship for Undergraduate Research *2012*

Activities

- Treasurer of American Association of Petroleum Geologists (AAPG) Southern Nevada Chapter (2015 – 2016)
- Member of AAPG
- National Society of Collegiate Scholars
- Phi Eta Sigma National Honor Society
- President of the Undergraduate Geology Club (2012 – 2013)
- McClung Museum Outreach